

Thin Conductive Films Sputtered on Anodized Aluminum
Substrates for Dye-Sensitized Solar Cell Fabrication

By

Marie-Pier Côté

A Thesis Submitted to the Faculty of Graduate Studies and Research in Partial
Fulfillment of the Requirements for the Degree of Master of Engineering
Department of Mining and Materials Engineering

McGill University

Montreal, Canada

August 2013

Abstract

The possibility of using aluminum as a substrate for dye-sensitized solar cells (DSCs) was studied. In order to do so aluminum coupons were anodized in oxalic acid and sputtered with a conductive thin layer of either titanium, molybdenum or indium-tin oxide (ITO). The titanium-coated substrates were used as anodes or cathodes in DSCs in pair with conductive glass electrodes. In turn the molybdenum and ITO-coated substrates were only used as cathodes. The efficiency of the DSCs and their stability were measured by irradiating them using a solar simulator calibrated to reproduce the irradiation of the sun at the Earth's surface. The maximum values of efficiency measured were 6.4%, 4.5% and 2.1% for titanium, molybdenum and ITO cells respectively. The high resistivity of the ITO sputtered film was found to be responsible for the low efficiency of these DSCs. The degradation of the overall conversion efficiency of titanium-based DSCs was studied over 10 days. It was found that the efficiency decreased with time partly due to the reaction of the electrolyte with the metallic electrode. The evaporation of the volatile electrolyte due to sealant limitations was also found responsible for part of the decrease in the efficiency.

Résumé

La possibilité d'utiliser l'aluminium comme substrat de cellules solaires à pigments photosensibles (DSCs) a été étudiée lors de ce projet de maîtrise. Pour ce faire des coupons d'aluminium ont d'abord été anodisés dans l'acide oxalique puis de minces films conducteurs de titane, de molybdène ou d'oxyde d'indium-étain (ITO) ont été déposés par pulvérisation cathodique. Les substrats de titane ont été utilisés en tant qu'anodes et en tant que cathodes dans des DSCs en pair avec des électrodes de verre conducteur. Les substrats de molybdène et de ITO quant à eux n'ont été utilisés que comme cathodes. L'efficacité de ces DSCs ainsi que leur résistance ont été mesurées en les irradiant à l'aide d'un simulateur solaire calibré pour reproduire l'irradiation du soleil à la surface de la Terre. L'efficacité maximale mesurée pour les cellules de titane, de molybdène et de ITO était de 6,4%, 4,5% et 2,1% respectivement. Il a été montré que la grande résistivité des films de ITO est responsable pour leur faible efficacité. La dégradation de l'efficacité des cellules à base de titane a été étudiée sur une période de 10 jours. Il a été montré que l'efficacité diminuait avec le temps, entre autre à cause de la réaction de l'électrolyte avec le substrat métallique. Une partie de cette diminution de l'efficacité est aussi attribuée à l'évaporation de l'électrolyte volatil.

Acknowledgements

I would love to acknowledge everybody who contributed to my masters from near and far but I am pretty sure that my memory will ensure to forget someone!

To start I would like to thank my two supervisors Professors Mathieu Brochu and George Demopoulos for the chance that they offered me, for their support and ideas and most importantly for their advices. Thanks to you I spent the last two years working on an amazing project, time during which I learned much more than I would ever have imagined. Thank you!

I would also like to acknowledge Nima and Nesli for introducing me to the world of solar cells and everything that it involves. Nima you were a great help throughout my project, thanks for answering to all my questions. Thanks to Prof Nate Quitariano for giving me the idea of sputtering and to Andrew for sputtering my first samples. Thanks to all the students of the NAIN lab: Jay, Rosen, Nesli, Dave Heard, Dave Walker, Gil, Sam, Cory, Sese, Jose, Masum, Phil, Rabab, Levasseur, Vicky, Franck and Javier. Thanks to the solar cells group: Nima, Nathan, Ivonne and Amrita. You were all of a great help!

Obviously the kind and helpful staff of McGill also deserves a round of applause. Thank you to M. Riendeau, R. Paquette, T. Zatylny, B. Hanley, L. Selway and C. Jelaco. I would also like to thank D. Berry, M. Nannini and L. Eugene from the McGill Nanotools – Microfab lab for their help with the sputtering of my samples (and changing the targets so often, right Don?).

Naturally, because you were certainly the best support I could have wished for, thank you mom, dad, Joe and all the family. Finally thanks to the “Shower Apple” members, to the “Rois Mages” and to my lovely roommates for being the most amazing friends!

Contributions of Authors and Co-Authors of Works Intended for Publication in this Thesis

M.-P. Cote, N. P. Benekohal, N. Alpay, G.P. Demopoulos and M. Brochu, "Titanium-Sputtered Anodized Aluminum Substrates". *Article intended for publication. 2013*

M.-P. Cote, G.P. Demopoulos and M. Brochu, "Molybdenum- and ITO-Sputtered Anodized Aluminum Substrates". *Article intended for publication. 2013*

In both articles intended for publication the first author conducted all the necessary characterization and produced all the material. N.P. Benekohal and N. Alpay helped producing and interpreting experimental results. Profs. Brochu and Demopoulos provided the funding and equipment for all materials and characterization and provided guidance for the elaboration of both publications.

The accuracy of the above statement is attested by the student's supervisors.

Table of contents

Abstract.....	2
Résumé	3
Acknowledgements	4
Contributions of Authors and Co-Authors of Works Intended for Publication in this Thesis	6
Table of contents	7
List of Figures	9
List of Tables	10
Chapter 1: Introduction	11
1.1 Motivation	11
1.2 Objectives.....	13
1.3 References.....	15
Chapter 2: Literature Review.....	16
2.1 Solar cells.....	16
2.2 Dye-sensitized solar cells.....	19
2.2.1 Operating mechanism of DSCs	20
2.2.2 DSC major components.....	23
2.2.3 DSC performance characterization.....	24
2.3 Metallic electrodes in DSCs	28
2.4 The use of aluminum.....	31
2.4.1 Anodization of aluminum.....	32
2.5 References.....	36
Chapter 3. Titanium-Sputtered Anodized Aluminum Substrates.....	40
3.1 Abstract	41
3.2 Introduction	42
3.3 Experimental	44
3.3.1 Aluminum substrate	44
3.3.2 Titanium sputtering.....	45
3.3.3 DSC fabrication	45
3.3.4 Microstructural and cell performance characterisation	47
3.4 Results & Discussion	48
3.4.1 Metallic electrodes characterisation.....	48
3.4.2 Efficiency analysis.....	49
3.4.3 Electrochemical impedance spectroscopy analysis.....	52
3.4.4 Analysis of cell performance over a 10-day period.....	55

3.4.5 Efficiency comparison	59
3.5 Conclusion.....	64
3.6 References	65
Chapter 4. Molybdenum- and ITO-Sputtered Anodized Aluminum Substrates	70
4.1 Abstract	71
4.2 Introduction	71
4.3 Experimental	73
4.3.1 Aluminum substrate	73
4.3.2 Conductive layer sputtering.....	74
4.3.3 DSC fabrication	74
4.3.4 Electrodes and DSC characterisation	76
4.4 Results & Discussion	77
4.5 Conclusion.....	83
4.6 References	84
Chapter 5. Summary	88
5.1 References	90

List of Figures

Figure 1.1: Global energy sources pie chart. (Adapted from [2])	12
Figure 2.1: Possible production costs per unit area (in year 2003) and efficiency ranges for the three generations of solar cells [4].....	18
Figure 2.2: Schematic of a DSC and the electron path in the cell.....	21
Figure 2.3: Schematic of the energy levels in a DSC.....	22
Figure 2.4: Typical DSC performance curve of J versus V	25
Figure 2.5: Solar radiation spectra out of the atmosphere and at sea level [15].....	26
Figure 2.6: Air Mass indices diagram [16].....	27
Figure 2.7: Metal roofing on a country house [35].....	31
Figure 2.8: Typical current vs. time curve for anodization at constant voltage (here 50V in 0.3mol/L oxalic acid solution) and the evolution of the anodic film structure [43].....	34
Figure 2.9: Schematic of the position of the original aluminum surface after anodizing (adapted from [41]).....	35
Figure 3.1: (a) front illumination and (b) back illumination configurations in which the TiO ₂ film is on the FTO-glass substrate and on the metal substrate, respectively.....	46
Figure 3.2: SEM cross-section of a metal substrate showing the 2 μ m thick porous alumina layer and the 1.1 μ m-thick sputtered titanium layer.....	49
Figure 3.3: I-V curves of DSCs based on 1.1 μ m- and 850nm-thick titanium films in FI and BI configurations. A 0.16cm ² mask was used for the measurements.....	52
Figure 3.4: Nyquist plots of front and back illumination DSCs based on a) 1.1 μ m- and b) 850nm-thick sputtered titanium substrates.....	54
Figure 3.5: Electrochemical impedance spectroscopy equivalent circuit.....	55
Figure 3.6: Efficiency degradation curves of the front and back illumination DSCs made with 1.1 μ m-thick sputtered titanium substrates and of the FI reference DSC made on FTO-glass electrodes. The efficiency values were measured without masking for consistency.....	58
Figure 3.7: SEM picture of a crack seen at the surface of an anodized aluminum coupon after heating at 450°C for 30 minutes.....	59
Figure 4.1: Schematic of the thin conductive film counter electrode-based DSC configuration.....	76
Figure 4.2: SEM picture of the cross-section of a molybdenum-sputtered anodized aluminum substrate showing the 2 μ m-thick alumina layer and the 1.2 μ m-thick molybdenum layer.....	78
Figure 4.3: Comparison of the I-V curves of ITO- and molybdenum-based front illumination configured DSCs.....	80
Figure 4.4: Nyquist plots of molybdenum- and ITO-based DSCs.....	81
Figure 4.5: Electrochemical impedance spectroscopy equivalent circuit.....	81

List of Tables

Table 2.1: Summary of the reaction of various metals with iodide/triiodide electrolyte.....	30
Table 3.1: Average efficiency data for 0.175cm ² masked area [40] DSCs mounted on titanium-sputtered anodized aluminum substrates or FTO-glass substrates at one sun illumination. A 0.16cm ² mask was used for the efficiency measurements. The outliers were removed from the statistics (2 outliers for BI and 1 outlier for FI, both for thin Ti film).	51
Table 3.2: Electrochemical impedance spectroscopy equivalent circuit resistance components R ₁ , DX1-C and R _s average values per DSC type, in ohms.....	55
Table 3.3: Comparison table of BI DSCs based on metallic electrodes. The Glass Ref column states the efficiency of the glass reference DSCs fabricated in the same studies whether it is “higher” or “lower” than the metal-based DSC. N/A in the masking area column indicates that this information was not mentioned.....	61
Table 3.4: Comparison table of FI DSCs based on metallic electrodes. The Glass Ref column states the efficiency of the glass reference DSCs fabricated in the same whether it is “higher” or “lower” than the metal-based DSC. N/A in the masking area column indicates that this information was not mentioned.	63
Table 4.1: Deposition conditions for molybdenum and ITO sputtering with Denton E14 DC.....	74
Table 4.2: Mo- and ITO-based DSCs short-circuit current (<i>J_{sc}</i>), open-circuit voltage (<i>V_{oc}</i>), fill factor (<i>FF</i>) and efficiency (<i>η</i>).	79
Table 4.3: <i>R_s</i> and <i>R₁</i> component of the equivalent circuit shown in Figure 4.5 for Mo- and ITO-based DSCs EIS.....	81

Chapter 1: Introduction

1.1 Motivation

In our days, electricity is an everyday life commodity in all developed countries. It allows us, for example, to have lighting on demand, to refrigerate, regulate the temperature in our homes and to use all types of electronic devices. But this access to electricity that is taken for granted in countries like Canada is not as easily available in other countries. In fact, one third of the world's population does not even have access to it [1]. As the life conditions in third-world countries is improving, the electricity and more generally the energy consumption increases radically. This adds up to the already increasing energy demand of industrialized countries like ours. It was evaluated in 2008 [2] that the total energy consumed on the planet by 2050 would be the equivalent of 270 cubic miles of oil (CMO) worth of energy. Knowing that only 120 CMOs of coal, 42 CMOs of natural gas and 46 CMOs of recoverable oil are estimated to be left in the world's reserve, without even considering the transformation issues, it is obvious that we are running towards challenging times.

As shown in the pie chart presented in Figure 1.1 [2], 87% of the world's energy consumption comes from oil, coal, nuclear and natural gas which are all non-renewable sources.

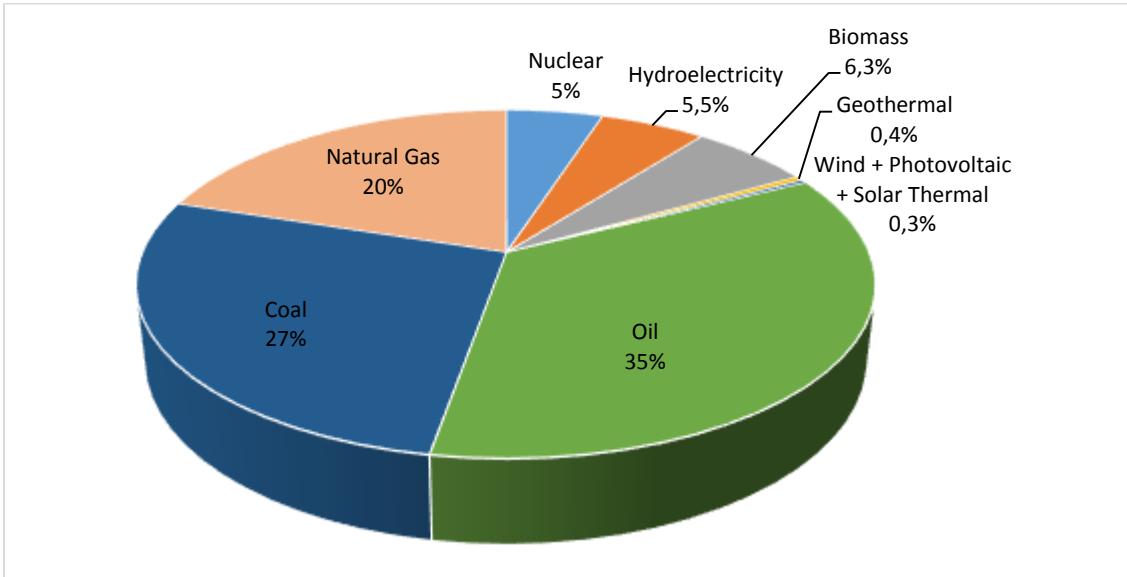


Figure 1.1: Global energy sources pie chart. (Adapted from [2])

In order to respond to the world's increasing demand in energy without destroying and emptying the planet, the global population will have to (1) change its consumption habits, and (2) increase the usage of renewable energy sources. A so-called renewable energy is by definition, an energy that was created using a source that can be renewed in a reasonable delay, meaning in months or in years at most [3]. Wind, sun, biomass, water and internal heat of the Earth are considered renewable energy sources. Being renewable, these sources provide a nearly unlimited supply of energy at a relatively low production price, which contributes to stabilizing the cost of energy.

Keeping in mind that the sun provides 10 000 times more raw energy than what we actually consume, one can easily see that photovoltaic (PV) technologies are part of the solution to this increasing demand.

1.2 Objectives

In order to include photovoltaic technologies in the solution to global warming and constantly increasing energy demands a lot of research is done to make solar cells more profitable, both economically and environmentally. This research focuses on the development of aluminum-based dye-sensitized solar cells. In that sense the main objectives of this work are the following:

- Fabrication of metallic electrodes based on electrically insulated aluminum and deposition of a thin conductive film by sputtering.
- Fabrication of front and back illumination DSCs using the new electrodes as counter-electrode and photo-electrode, respectively.
- Characterization of the performance of the metal-based DSCs in terms of overall conversion efficiency.
- Investigation of the stability of the metal-based DSCs in time.

This thesis is presented as a manuscript based thesis with two primary investigations intended for publication in open literature. The first publication, presented in Chapter 3, reports the performance of DSCs based on titanium-

sputtered substrates with two titanium thicknesses and two configurations. A study of the degradation of the DSCs is also presented in Chapter 3. The second publication, presented in Chapter 4, studies DSCs with the same configuration as the ones presented in the first publication but based on ITO and molybdenum sputtered films.

1.3 References

1. K. Hara and H. Arakawa, Handbook of Photovoltaic Science and Engineering. John Wileys & Sons, New York (2011), p.1-38.
2. <http://www.energyandcapital.com/articles/future-sources-energy/787>
3. L'ABC des Technologies de l'Énergie Renouvelable. See www.pollutionprobe.org/report/reprimerfr.pdf.

Chapter 2: Literature Review

2.1 Solar cells

Although solar cells might seem like a new technology, their history goes all the way back to the nineteenth century. As a matter of fact, the first intentional and functional PV device was fabricated by Fritts in 1883 [1]. In spite of this, it was only in 1954 that the modern era of PV began, when researchers at Bell Labs discovered that *pn* junction diodes generated a voltage when they were left under the room lights. This accidental discovery allowed them to produce a 6% efficient Si *pn* junction solar cell within a year [2]. Since then the amount of research done on PV devices has increased constantly, focussing on various aspects of their functionality, such as improving their energetic performance, the manufacturing economics and their environmental footprint. In 1999, 25 years after the installation of the first PV device, the cumulative worldwide functional PV devices reached 1000 MW. Only 3 years later this number was doubled. Hence, only between 1998 and 2008, the PV market has increased by 20 folds, and this number keeps increasing.

Solar cells have been categorized in 3 different generations. The first generation includes the silicon-based solar cells, which comprises monocrystalline, polycrystalline, amorphous and hybrid silicon cells. This generation, which is the

oldest, takes over 80% of the solar cell market [3]. However the situation might change as forthcoming generation of solar cells were/are becoming cheaper and more efficient. The second generation includes thin-film and building integrated technology. A wider range of type of semiconductor used in these solar cells and it goes from silicon to cadmium telluride and to copper-indium-gallium-selenide. As of today, their efficiency remains lower than that of silicon cells, but interest remains as they possess other major advantages. They are thinner, which represents an economical advantage when compared to the use of silicon wafers since less semiconductor material is required. The size of an actual unit can be greatly increased, as their size is no longer limited by the size of a silicon wafer (~100cm²) but by that of a glass sheet (~1m²), so an area gain of about 100 times [4]. Yet, their efficiency remains lower than the silicon-based cells. In fact, the National Renewable Energy Laboratory (NREL) reported at the end of 2010 that the best laboratory efficiency published for 1st generation cells was 27.6% and 20.3% for 2nd generation cells [5]. As with everything, the continuous research ongoing on these solar cells should yield an increase in efficiency, which should close the gap with the silicon-based first generation systems.

The third generation of solar cells are still, for most, at the laboratory phase. Although they suffer from fast degradation and low efficiencies, this generation of

cells is very promising, especially in terms of production costs and theoretical efficiencies [4]. This generation includes dye-sensitized solar cells (DSCs), the topic of this thesis.

Figure 2.1 compares the possible production costs per unit area along with the energy conversion efficiency ranges for the three generations aforementioned.

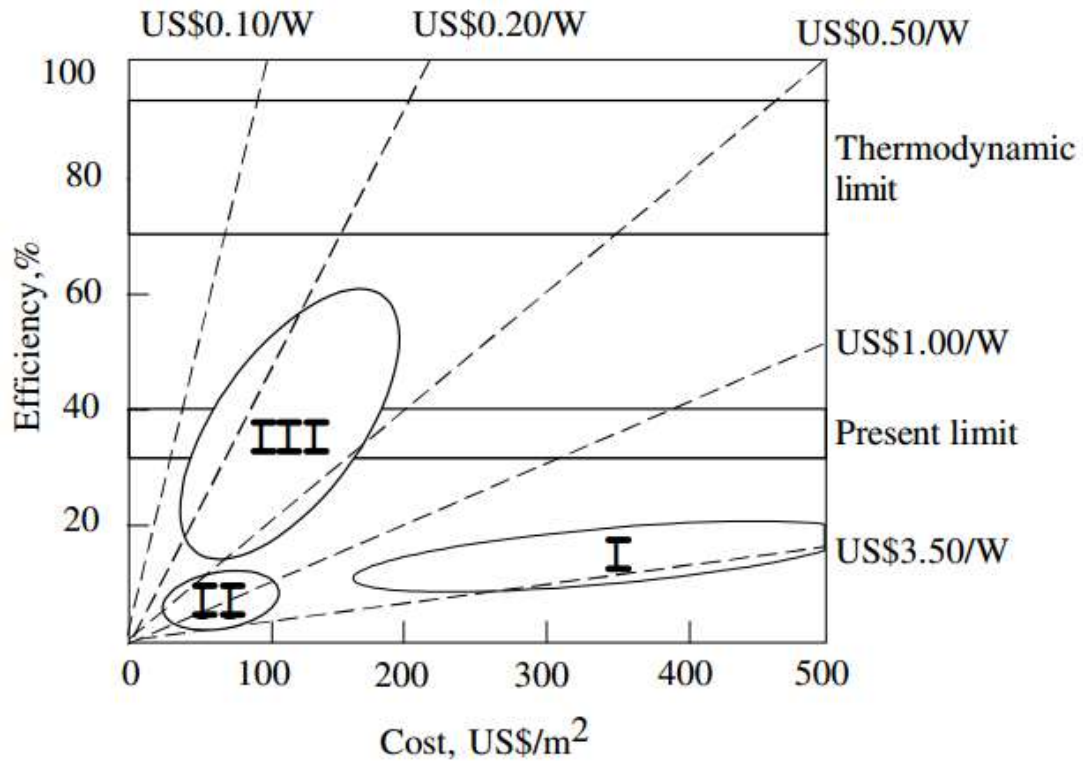


Figure 2.1: Possible production costs per unit area (in year 2003) and efficiency ranges for the three generations of solar cells [4].

2.2 Dye-sensitized solar cells

In 1991, O'Regan and Grätzel produced the first DSC, a solar cell based on a nanosized TiO₂ film sensitized using a new ruthenium-complex sensitizer capable of absorbing light from the visible and near-IR region, from 400 to 800nm [6]. An initial efficiency of 7% was reported and has now increased to more than 11% [7] through optimizing the structure of the various cells components. These results favored the emergence of new companies like G24i (United Kingdom), Dyesol (Australia) and Solaronix (Switzerland) that provide the primary materials necessary for the fabrication of DSCs. The improvement in efficiency also led to the development of a first generation of derived products such as portable battery charging items like sports bags, backpacks, blankets, etc. Nowadays, system integrated DSCs are extensively studied. As an example the companies Dyesol and Tata Steel have joined their efforts to develop a new stainless steel based DSCs for building integrated applications [8].

DSCs present many advantages, which make them an attractive alternative to the common silicon-based cells. Specifically, they can perform under low light irradiance and they can be made light weight, thin and flexible when fabricated on specific substrates (topic to be discussed later). Their most interesting particularity

is their expected low production costs because the cells are made of low-cost materials and are simple to assemble [7].

2.2.1 Operating mechanism of DSCs

DSCs, like any other solar cells, are devices that use the light irradiation to produce a flow of electrons. Their operation resembles that of the natural photosynthesis phenomenon achieved by plants. The energy conversion mechanism is very different to the semiconductor-based solar cells. It is based on the principle that the light absorption and the charge carrier transport mechanisms are taken in charge by two different components of the cells. Figure 2.2 shows a schematic of the sandwich-like configuration of a DSC and presents the path of the electrons in the cell.

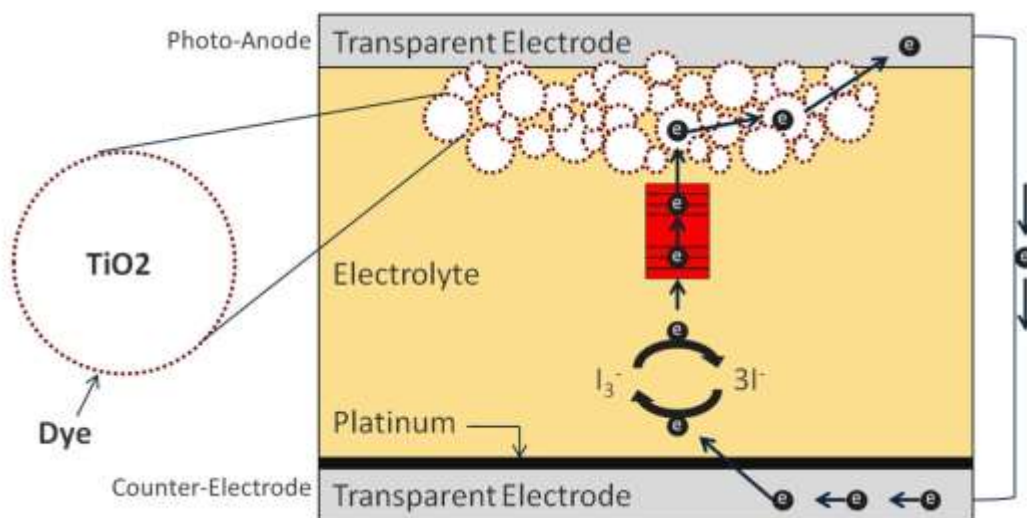


Figure 2.2: Schematic of a DSC and the electron path in the cell.

Typical DSCs are composed of a photoanode, a counter-electrode and a redox electrolyte. The photoanode consists of a thin nano-porous TiO_2 film deposited on a transparent conductive glass substrates and sensitized using an organometallic dye. The counter-electrode consists of a platinized transparent conductive glass substrate. When the photoanode is irradiated by a light source the dye molecule absorbs an incident photon and is excited from the ground state (S) to the excited state (S^*) following Reaction 2.1. This causes an electron of the HOMO level of the dye to jump to the LUMO level (Figure 2.3, 1), this electron is then injected in the TiO_2 conductive network following Reaction 2.2. Then the injected electron diffuses towards the TCO layer of the photoanode substrate (figure 2.3, 2) and further to the platinized counter-electrode through an external load (Figure 2.3, 3).



The role of the electrolyte is to regenerate the ground state of the dye by injecting electrons into its HOMO level (Figure 2.3, 4). The electrons are generated by the oxidation of I^- to I_3^- ions which then diffuse to the counter-electrode surface where they are reduced back to I^- ions using the electrons originally injected by the excited dye molecules (Figure 2.3, 5). Overall the DSC produces electric current without suffering any permanent chemical damage.

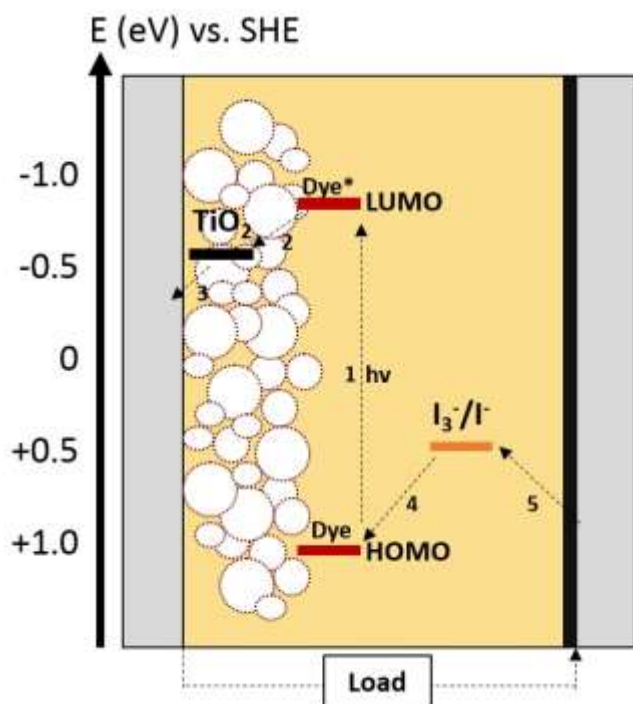


Figure 2.3: Schematic of the energy levels in a DSC.

2.2.2 DSC major components

- The transparent conductive electrode substrates are typically transparent conductive oxides (TCO)-coated glass substrates; the TCO is generally indium-tin oxide (ITO) or fluoride-doped tin oxide (FTO).
- The photoanodes of this study were fabricated using a commercial TiO₂ paste from Dyesol (18NRT). The resulting film is transparent and the size of each particle ranges between 10 and 20nm. It is this small dimension that provides the high surface area to the film allowing the absorption of a maximum of dye molecules. A thin layer of bigger TiO₂ particles is sometimes applied on top of the transparent layer for scattering properties.
- The dye used for this work is a ruthenium (II) complex made of as cis-(di-thiocyano)bis(2,2'-bipyridil-4,4'-dicarboxylic acid) commercially known as N719. This dye with absorption properties in the visible (450-600nm) and near-IR (920nm) was developed by Gratzel's group [9]. Even if it is the most widely used dye other ruthenium (II) sensitizers have been developed [10] such as the black dye which made achieving a conversion efficiency of 10.4% possible.
- The electrolyte is usually made of an organic solvent containing a redox mediator system, in this case iodide and triiodide. Lately, iodide-free [11, 12] and solid-state [13, 14] electrolytes have been developed to overcome

the corrosion and evaporation problems encountered with the iodide-based electrolyte.

2.2.3 DSC performance characterization

The performance of a DSC is characterized by its short-circuit current density (J_{sc}) which is the maximum current that can flow between the anode and the cathode and the open-circuit voltage (V_{oc}) which is a measure of the maximum potential difference that can be provided by the cell. The fill factor (FF) is another important parameter that is defined as the ratio of the maximum achievable power to the theoretical power as expressed in Equation 2.1.

$$FF = \frac{V_{MP} * I_{MP}}{V_{OC} * I_{SC}} = \frac{P_{max}}{P_{theoretic}} \quad \text{Equation 2.1}$$

The variables V_{MP} and I_{MP} in Equation 2.1 stand for the potential and the current yielding the maximum power as illustrated in Figure 2.4.

Most importantly, DSCs are characterized by their overall conversion efficiency (η). This efficiency value is defined as the ratio of the maximum achievable power of the solar cell to the power of the incident light as expressed in Equation 2.2.

$$\eta = \frac{P_{\max}}{P_{\text{light}}} \quad \text{Equation 2.2}$$

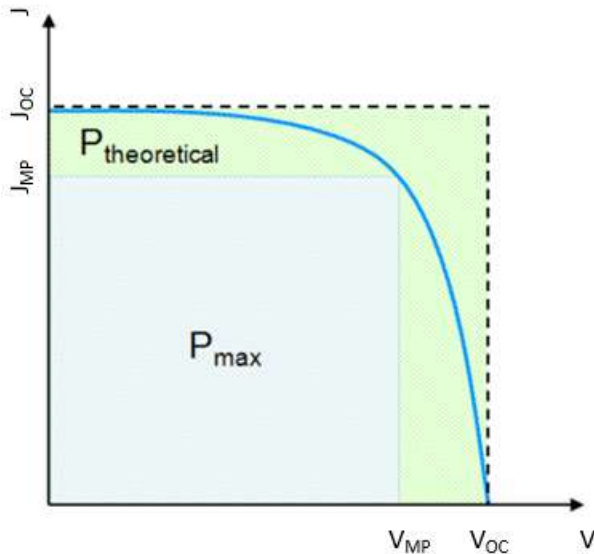


Figure 2.4: Typical DSC performance curve of J versus V .

A curve such as the one presented in Figure 2.4 is measured by irradiating the solar cell with a calibrated light source simulating the sun light with a power of $1000\text{W}/\text{m}^2$ which is the power received at sea level absorption by the atmosphere. Figure 2.5 illustrates the irradiance spectrum of the sun at sea level. By convention an Air Mass index of 1.5 (AM 1.5) is used. This index relates to the spectral energy

distribution of the light: an index of 1 is associated to a 0° incidence angle whereas Air Mass 1.5 is associated to the light received by locations situated at latitudes between 30° and 60° as shown in Figure 2.6.

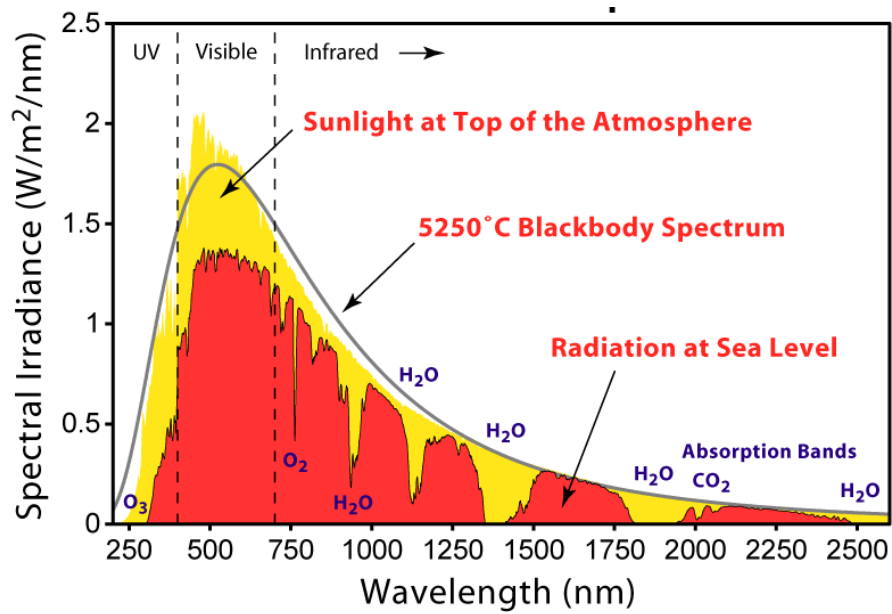


Figure 2.5: Solar radiation spectra out of the atmosphere and at sea level [15].

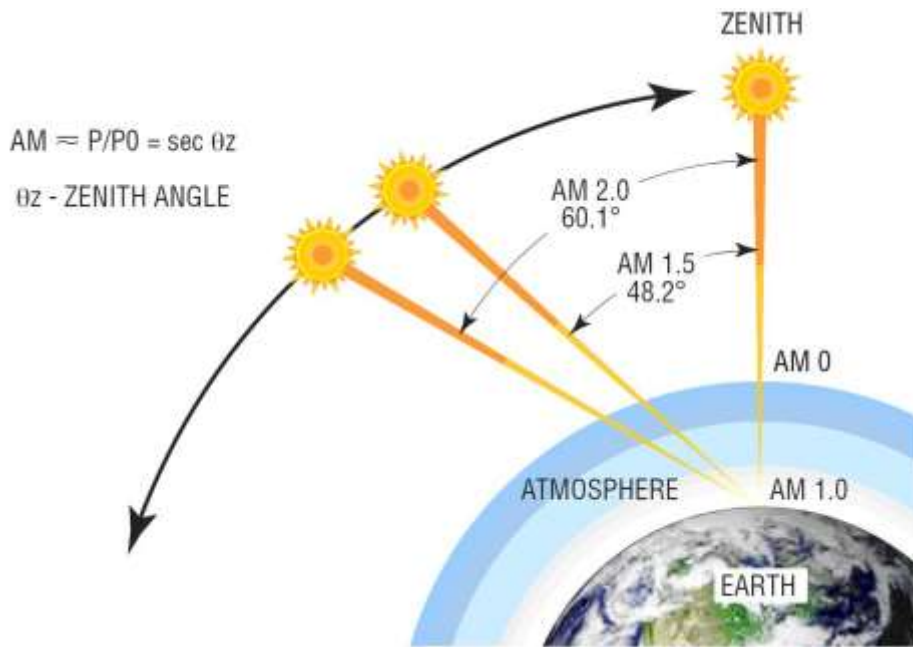


Figure 2.6: Air Mass indices diagram [16].

Typically, the DSC is masked to expose only a section of the active area of the cell when measuring its performance. For non-commercially fabricated cells, imperfections located at the edge of the TiO₂ film can be present and the fact of masking the cell for measurements will increase the efficiency by eliminating the poor contribution of these defects. However, masking the cell properly includes masking the edges of the cell, thus eliminating any possible refraction of the incident light through the edges. Therefore, for a large-area DSC or for high-quality TiO₂ films, masking can reduce the measured efficiency. Nevertheless, the accepted approach of masking the cell is accepted for comparison between DSCs performance.

2.3 Metallic electrodes in DSCs

As mentioned previously, DSCs possess the possibility of being flexible (to a certain extent) with the usage of non-rigid substrates. Moreover, it was stated by J.M. Kroon [17] that TCO-glass constitutes about one third of the material costs of DSCs. These substrates are also the DSCs component that is the most detrimental to the environment (production wise). Since DSCs and solar energy are seen as green concepts, the ecological footprint is another reason to find an alternative to TCO-glass. Because of all these reasons many research groups have focused their work on changing the commonly used TCO-glass by different polymers [18-24] and metallic substrates [18, 19, 25-34] such as stainless steel, nickel, copper, aluminum, titanium and zinc. Although the metals included in this list have been studied for DSC applications, they do not all qualify, mostly because of the possible reaction of the electrolyte with the different metallic substrate.

Table 2.1 reports results of four studies focusing on the reaction of the iodide-based electrolyte with various metals. The first conclusion to be drawn from Table 2.1 is that stainless steel, titanium and Inconel could potentially be used as DSCs electrodes because of their good corrosion resistance in the iodide-based electrolyte. Oppositely, aluminum, iron, molybdenum, copper and zinc were found to react with the electrolyte. When such a reaction happens a color change can be

seen as the electrolyte goes from dark orange to pale yellow or colorless. Since the triiodide ions are responsible for the orange color of the electrolyte and because iodide ions are colorless this change in color is attributed to the reduction of triiodide ions. It was proposed by M. Toivola et al. [31] that the triiodide ions present in the solution could react with the metal substrates to be reduced to iodide ions following Reaction 2.3.



Since the reduction/oxidation reactions in the electrolyte are necessary for the regeneration of the ground state of the dye molecules, the reduction of the concentration of triiodide ions is responsible for a slower regeneration rate and ultimately a lower overall conversion efficiency.

Table 2.1: Summary of the reaction of various metals with iodide/triiodide electrolyte.

Authors	Metal(s) studied	Type of test(s)	Conclusion
J. Wei et al. [30]	<ul style="list-style-type: none"> ▪ Aluminum film 	<ul style="list-style-type: none"> ▪ DSCs fabrication 	<ul style="list-style-type: none"> ▪ Reaction with the electrolyte in the presence of platinum
G.J. Reynolds et al. [34]	<ul style="list-style-type: none"> ▪ Molybdenum ▪ Titanium ▪ Stainless Steel ▪ Iron ▪ Aluminum 	<ul style="list-style-type: none"> ▪ Encapsulation 	<ul style="list-style-type: none"> ▪ Al and Fe react with the electrolyte within 20 hours. ▪ Mo reacts after 8 weeks. ▪ Ti and StS were stable for more than 12 weeks.
M. Toivola [31]	<ul style="list-style-type: none"> ▪ Carbon Steel ▪ Zinc-coated Carbon Steel ▪ Stainless Steel ▪ Copper 	<ul style="list-style-type: none"> ▪ Soaking ▪ Encapsulation tests 	<ul style="list-style-type: none"> ▪ StS and C-steel were stable in the electrolyte for several months. ▪ Zn-coated C-steel and Cu react with the electrolyte.
K. Miettunen et al. [32]	<ul style="list-style-type: none"> ▪ Stainless Steel ▪ Inconel ▪ Titanium 	<ul style="list-style-type: none"> ▪ DSC fabrication 	<ul style="list-style-type: none"> ▪ All three metals were stable in the electrolyte.

The most obvious application of metal-based DSCs is the fabrication of building integrated devices. In that case the metal used to cover surfaces exposed to the sun would be used as a substrate for solar cells, thus adding functionality to the already existing base material. An example of possible application of building integrated DSCs is shown in Figure 2.7, where a house with a metal-covered roof is shown. In this case, the roof could have been covered with metal-based solar panels directly instead of using passive metal claddings.



Figure 2.7: Metal roofing on a country house [35].

2.4 The use of aluminum

Due to its chemical reactivity aluminum was not extracted as an industrial metal until 1886 but as of this year the world production of aluminum rapidly grew and reached 203 kilotonnes in 1921. As aluminum continued to take its place in the industry this number had increased to 17.8 million tonnes by 1988 and aluminum is now the second most widely used metal, right after steel [36]. The popularity of aluminum is mainly related to its low density of 2.7g/cm^3 , one third that of steel, its good corrosion resistance and the possibility of coloring it. Although pure aluminum in the fully annealed condition is soft its strength can be increased substantially by alloying, strain hardening, solid-solution hardening or precipitation hardening among others techniques providing it a good specific strength. In terms of

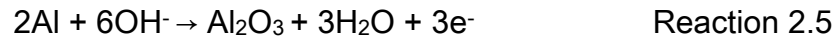
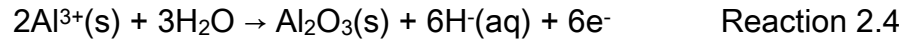
corrosion aluminum owes its resistance to the naturally forming alumina layer on its surface. Typically this layer is about 2-3nm in thickness [37] but an electrochemical process can be applied to the surface in order to increase the thickness of the protective film to tenths of nanometers. Because of these characteristics, aluminum has become an excellent choice for outdoors applications, which makes it an attractive substrate for building integrated DSCs.

2.4.1 Anodization of aluminum

Anodization is an electrochemical process that forms a highly ordered quasi periodic hexagonal nanostructured structure at the surface of aluminum [38-40]. This layer is known to improve the corrosion resistance of the aluminum, increase its wear resistance and provide better adhesion properties than the metal alone. Moreover it is stronger and more adherent than most paint and other metal plating.

During anodizing, the aluminum, which is the anode in the electrochemical circuit, is immersed in an electrolytic solution along with a cathode. A continuous current is applied between the two electrodes through the electrolyte releasing hydrogen at the cathode and oxygen at the anode. Although anodization of aluminum has been studied extensively it is not clear yet which oxygen-carrying anion species

are involved in the anodic process, O^{2-} or OH^- ions. Thus the growth of the oxide film is believed to follow Reaction 2.4 and either Reaction 2.5 or Reaction 2.6 [41].



Three major steps take place during the anodizing process, and are depicted in Figure 2.8. Firstly, the high initial current density caused by the oxygen evolution at the surface of aluminum (Figure 2.8a) drops rapidly because of the formation of the highly resistive oxide layer at the surface (Figure 2.8b). This phase is very short, usually happening within 5 to 10s [42]. Secondly local dissolution of the alumina layer initiates at the oxide/electrolyte interface (Figure 2.8c) which leads to the formation of vertical pores (Figure 2.8d). This dissolution of the oxide layer is accompanied by a gradual increase in the current density until it saturates and reaches a constant value. At this point the dissolution and growth mechanisms have reached an equilibrium state and the thickness of the porous alumina layer increases with time. In the end, the final porous layer will have grown under the original aluminum surface, as illustrated by Figure 2.9.

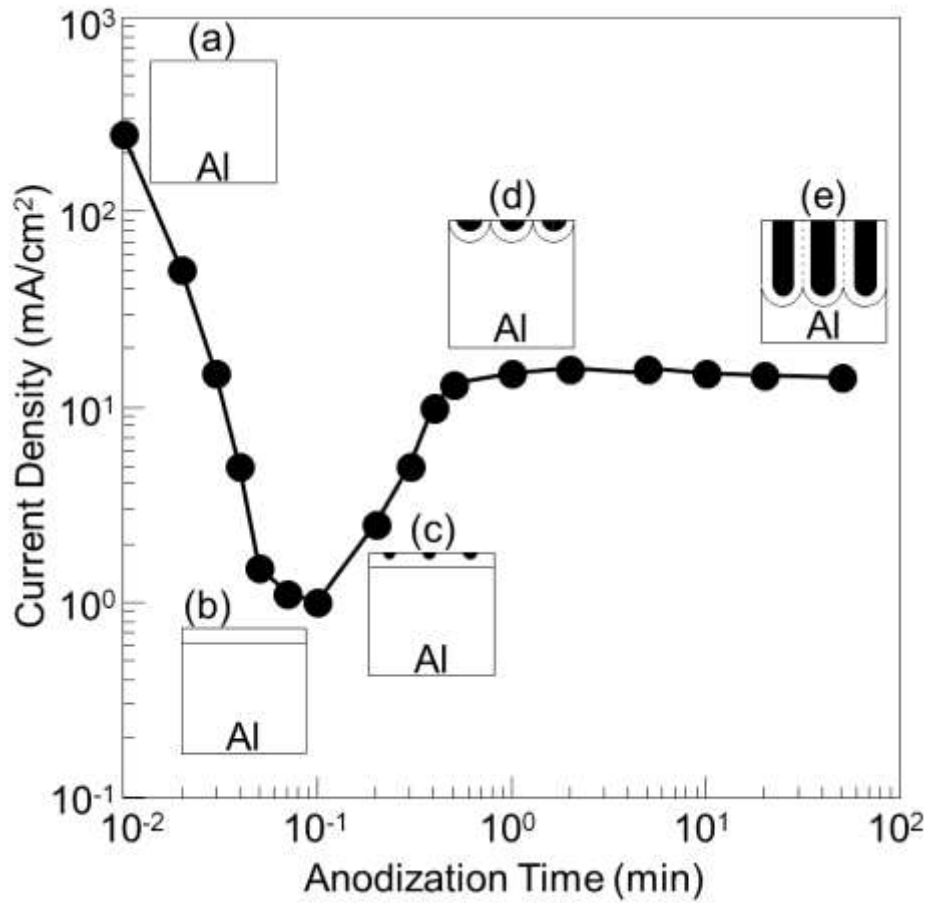


Figure 2.8: Typical current vs. time curve for anodization at constant voltage (here 50V in 0.3mol/L oxalic acid solution) and the evolution of the anodic film structure [43].

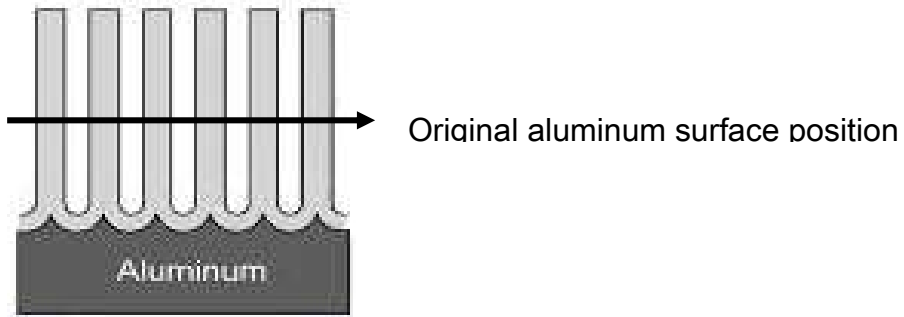


Figure 2.9: Schematic of the position of the original aluminum surface after anodizing (adapted from [41]).

2.5 References

1. K. Hara and H. Arakawa, Handbook of Photovoltaic Science and Engineering. John Wileys & Sons, New York (2003), p.1-44.
2. D.M. Chapin, C.S. Fuller and G.L. Pearson. A new silicon p-n junction photocell for converting solar radiation into electrical power. Journal of Applied Physics 1954; 25: 676.
3. L.M. Peter. Towards sustainable photovoltaics: the search for new materials 2011; 369: 1840.
4. M.A. Green, Third Generation Photovoltaics Advanced Solar Energy Conversion. Springer, Berlin (2006), p.1-6.
5. L. L. Kazmerski. National Renewable Energy Laboratory (NREL), Golden, CO.
6. B. O'Regan and M. Gratzel. A low-cost, high-efficiency solar-cell based on dye-sensitized colloidal TiO₂ films. Nature 1991; 353: 737.
7. K. Hara and H. Arakawa, Handbook of Photovoltaic Science and Engineering. John Wileys & Sons, New York (2011), p.642-674.
8. Tata Steel. 2011 Sustainable energy solutions. See http://www.tatasteeleurope.com/en/responsibility/sustainable_solutions/energy/.
9. A. Hagfeldt and M. Gratzel. Light-induced redox reactions in nanocrystalline systems. Chemical Reviews 1995; 95: 49.
10. M. Gratzel. Recent advances in sensitized mesoscopic solar cells. Accounts of Chemical Research 2009; 42: 1788.
11. J.-H. Yum et al. A cobalt complex redox shuttle for dye-sensitized solar cells with high open-circuit potentials. Nature Communications 2012; 3: 1.
12. M. Wang et al. An organic redox electrolyte to rival triiodide/iodide in dye-sensitized solar cells. Nature Chemistry 2010; 2: 385.
13. J.K. Koh et al. Highly efficient, iodine-free dye-sensitized solar cells with solid-state synthesis of conducting polymers. Advanced Materials 2011; 23: 1641.

14. I.Chung et al. All-solid-state dye-sensitized solar cells with high efficiency. Nature 2012; 485: 486.
15. <http://org.ntnu.no/solarcells/pages/Chap.2.php>
16. <http://www.optoiq.com/index/photronics-technologies-applications/lfw-display/lfw-article-display/361941/articles/laser-focus-world/features/photovoltaics-measuring-the-sun.html>
17. J.M. Kroon et al. Nanocrystalline dye-sensitized solar cells having maximum performance. Progress in Photovoltaics: Research and Applications 2007; 15: 1.
18. M. Ikegami et al. Platinum/titanium bilayer deposited on polymer film as efficient counter electrodes for plastic dye-sensitized solar cells. Applied Physics Letters 2007; 90: 153122-1.
19. T. Ma et al. Properties of several types of novel counter electrodes for dye-sensitized solar cells. Journal of Electroanalytical Chemistry 2004; 574: 77.
20. W.A. Gazotti et al. Flexible photoelectrochemical devices based on conducting polymers. Synthetic Metals 2000; 108: 151.
21. H. Lindstrom et al. A new method to make dye-sensitized nanocrystalline solar cells at room temperature. Journal of Photochemistry and Photobiology A: Chemistry 2001; 145: 107.
22. G. Boschloo et al. Optimization of dye-sensitized solar cells prepared by compression method. Journal of Photochemistry and Photobiology A: Chemistry 2002; 148: 11.
23. C. Longo et al. Solid-state and flexible dye-sensitized TiO₂ solar cells: a study by electrochemical impedance spectroscopy. Journal of Physical Chemistry B 2002; 106: 5925.
24. C. Longo, J. Freitas and M.-A. De Paoli. Performance and stability of TiO₂/dye solar cells assembled with flexible electrodes and a polymer electrolyte. Journal of Photochemistry and Photobiology A: Chemistry 2003; 159: 33.

25. K. Miettunen, J. Halme and P. Lund. Segmented cell design for improved factoring of aging effects in dye solar cells. *Journal of Physical Chemistry C* 2009; 113: 10297.
26. T.M. Watson, G.J. Reynolds and D.A. Worsley. Painted steel mounted dye sensitised solar cells: titanium metallisation using magnetron sputtering. *Ironmaking and Steelmaking* 2011; 38: 168.
27. Y. Jun, J. Kim and M.G. Kang. A study of stainless steel-based dye-sensitized solar cells and modules. *Solar Energy Materials & Solar Cells* 2007; 91: 779.
28. C.-M. Chen, C.-H. Chen and T.-C. Wei. Chemical deposition of platinum on metallic sheets as counterelectrodes for dye-sensitized solar cells. *Electrochimica Acta* 2010; 55: 1687.
29. S. Ito et al. High-efficiency (7.2%) flexible dye-sensitized solar cells with Ti-metal substrate for monocrystalline-TiO₂ photoanode. *Chemical Communications* 2006: 4004.
30. J. WeiWei et al. A new type counter electrode for dye-sensitized solar cells. *Science in China Series E: Technological Sciences* 2009; 52: 1923.
31. M. Toivola, F. Ahlskog and P. Lund. Industrial sheet metals for nanocrystalline dye-sensitized solar cell structures. *Solar Energy Materials & Solar Cells* 2006; 90: 2881.
32. K. Miettunen et al. Stability of dye solar cells with photoelectrode on metal substrates. *Journal of the Electrochemical Society* 2010; 157: B814.
33. J.H. Park et al. Fabrication of an efficient dye-sensitized solar cell with stainless steel substrate. *Journal of the Electrochemical Society* 2008; 155: F145.
34. G.J. Reynolds et al. Corrosion resistance of metallic substrates for the fabrication dye-sensitized solar cells. *Journal of the Electrochemical Society* 2011; 33: 129.
35. www.demyanroofing.com

36. www.aluminum.org
37. P.G. Sheasby and R. Pinner, *The Surface Treatment and Finishing of Aluminum and its Alloys* (6th edition). ASM International and Finishing Publications (2001), p.1-1387.
38. H. Masuda and K. Fukuda. Ordered metal nanohole arrays made by a two-step replication of honeycomb structure of anodic alumina. *Science* 1995; 268: 1466.
39. W. Lee et al. Fast fabrication of long-range ordered porous alumina membranes by hard anodization. *Nature Materials* 2006; 5: 741.
40. K. Nielsch et al. Self-ordering regimes of porous alumina: the 10 porosity rule. *Nano Letters* 2002; 2: 677.
41. *Nanostructured Materials in Electrochemistry*. Wiley-VCH, Weinheim (2008), p. 1-186.
42. P. Chowdhury et al. Effect of process parameters on growth rate and diameter of nano-porous alumina templates. *Bulletin of Materials Science* 2011; 34: 423.
43. T. Ohgai. *Nanowires Recent Advances*. Intech (2012), p.101-125.

Chapter 3. Titanium-Sputtered Anodized Aluminum Substrates

In this chapter formatted in the form of a manuscript for publication titanium is sputtered as a thin conducting coating on previously anodized aluminum coupons for the purpose of investigating electrodes for dye-sensitized solar cell applications. The titanium-sputtered anodized aluminum substrates are characterized and then assembled into devices. The latter are tested in terms of photovoltaic performance and analysed with the aid of electrochemical impedance spectroscopy. Finally the devices are subjected to preliminary stability testing.

This chapter is intended for submission to a journal in the near future. The following provides the current citation information:

M.-P. Cote, N. P. Benekohal, N. Alpay, G.P. Demopoulos and M. Brochu, "Titanium-Sputtered Anodized Aluminum Substrates". *Article intended for publication. 2013*

3.1 Abstract

Metallic electrodes have already been used in DSCs to replace glass-based electrodes thus providing a certain flexibility to the cells. One of the most commonly used metal is stainless steel and it has been shown that stainless steel is a suitable electrode substrate for DSCs applications. In this study anodized aluminum coupons were sputtered with titanium and successfully used as DSCs electrodes substrates. Thicknesses of titanium of 850nm and 1.1 μ m were studied and front- and back-illumination DSCs were fabricated in the scope of this study. The characterization of the photovoltaic performance of the cells shows that the maximum efficiency of DSCs fabricated in the same configuration is not influenced by the thickness of the titanium film. On the other hand the efficiency is significantly higher for front-illumination DSCs than for back-illumination devices. A maximum efficiency of 6.4% was achieved on front-illumination DSCs whereas a maximum efficiency of 3.1% was measured on the back-illumination DSCs. A significant reduction of the efficiency of all the DSCs over a period of 10 days is seen which results from the evaporation of the liquid electrolyte and its reaction with the aluminum substrate.

3.2 Introduction

Dye-sensitized solar cells (DSCs) have attracted a lot of attention in the recent years because of their relatively high theoretical light-to-electricity conversion, their potentially low production costs and simplicity in fabrication [1-7] that does not require complex and energy intensive high temperature vacuum processes. Moreover, although conventional silicon solar cells currently exhibit a higher efficiency than DSCs [8] their need of direct sunlight radiation and the use of expensive and easily broken tracking systems represent a major disadvantage when compared to DSCs. Furthermore, the most attractive advantage of DSCs over silicon cells remains the possibility of fabricating building-integrated and non-flat devices. A lot of research has been done in that direction in order to replace the flat and brittle conventional glass electrodes used in DSCs by either polymeric [9-13] or metallic [14-25] electrodes. Moreover, the transparent conductive oxide (TCO)-glass typically used in DSCs represents a major part of their cost [6,26] and is the component that has the largest negative impact on the environment due to its complex fabrication process [5,27]. Thus, the alternative in replacing the use of TCO glass by metallic electrodes to make DSCs more profitable, both economically and environmentally, becomes extremely attractive.

Although the use of metallic electrodes is economically and environmentally advantageous, their reaction with the iodide/triiodide electrolyte is a major issue

that remains to be dealt with. Many studies have been conducted in order to discriminate the metals that are resistant to a reaction with the electrolyte [15, 21-23, 25]. Of the metals studied titanium [23, 25], stainless steel [15, 22, 23, 25] and Inconel [23] were found to be stable in the presence of the electrolyte. Oppositely polished aluminum coupons were found to be very reactive in the same conditions, reacting with the electrolyte within only 4 hours [25].

Building integrated photovoltaics is a steadily improving technology [28] and DSCs are now developed for entering this market. On the other hand, aluminum which comes in second rank of the most widely used materials [29, 30] and more than often used in sun-exposed outdoor application (window frames, building side panels, etc...) is almost entirely absent from the DSC industry. In addition to the corrosion problem cited above, another reason could emanate from the fact that aluminum is generally anodized before being used for building purposes. The alumina layer produced by anodization has a high electrical resistance which would prevent conduction both through the alumina layer and towards the aluminum substrate if an attempt was made for electrode usage. Nevertheless, just in Western Europe 200 000 tonnes of rolled aluminum have been used for building applications in 2006 and this number keeps increasing [31]. This volume of aluminum, which in part is exposed to the sunlight could be exploited if a proper technology permitting the coupling of aluminum and DSCs could be developed.

In this study, a different aluminum-based electrode design has been proposed, which aims to overcome the corrosion and electrical resistance issues. The concept lies in thin film surface engineering, where the aluminum substrates were first anodized, followed by sputtering of a titanium layer used as a conduction layer, mimicking the transparent conductive oxide glass concept. These electrodes have been used both as counter-electrodes and photo-anodes paired with FTO-glass electrodes. This paper reports the fabrication steps and the photovoltaic characteristics of these titanium-sputtered anodized aluminum-based DSCs.

3.3 Experimental

3.3.1 Aluminum substrate

A 3.2mm-thick AA 1100 plate was used as the base material for the electrode substrate. Samples of 4.5cm by 2.5cm in dimension were first ground down to 1200 grit grinding paper in order to eliminate surface defects created during rolling and handling. The samples were then pre-treated by dipping in a 2.5M sodium hydroxide solution at 55°C for 30 seconds to remove the native aluminum oxide layer and subsequently dipping in a 2.4M nitric acid at room temperature for 30 seconds to improve the surface finish. The samples were rinsed with water and

methanol and dried after each pre-treatment step. The pre-treated samples were then anodized over a 9cm² area in 0.3M oxalic acid at 20°C under a potential of 30V for 30 minutes.

3.3.2 Titanium sputtering

The anodized aluminum substrates were cleaned with methanol prior to sputtering.

The titanium thin films, serving as current carrier for the cell, were deposited using a Denton E14 DC sputterer in an argon atmosphere at 8mTorr at room temperature. The current used was 0.6A resulting in a deposition rate of approximately 1.75Å/s. Two final thicknesses were targeted: 850nm and 1.1µm.

The actual thicknesses were determined by measuring the film thickness on a glass dummy sample using a stylus profilometer and the reported values are an average of 10 samples. These anodized-aluminum substrates sputtered with titanium will simply be called metal substrates from now on.

3.3.3 DSC fabrication

Prior to the cell fabrication, holes were drilled in the fluorine-tin oxide (FTO)-glass substrates which were then cleaned with micro-90 soap in an ultrasonic bath for

30 minutes and further rinsed with ethanol and dried. The metal substrates were simply wiped with ethanol.

A 50 μm thick mask with an area of 1 cm^2 was applied on the conductive surface of the photo-anode substrates, either FTO-glass or metal substrates depending on the configuration used as shown on Figure 3.1. A TiO_2 paste (Dyesol 18NRT) was applied using the doctor blading technique and sintered at 450 $^\circ\text{C}$ for 30 minutes after removal of the mask. The thickness of the TiO_2 films was measured using a stylus profilometer and only the anodes with a TiO_2 film thickness between 8 and 12 μm were further used. Finally, the anodes were immersed in a ruthenium-based dye (N719, Dyesol) for 24h. The now sensitized anodes were rinsed with ethanol and dried and were assembled immediately.

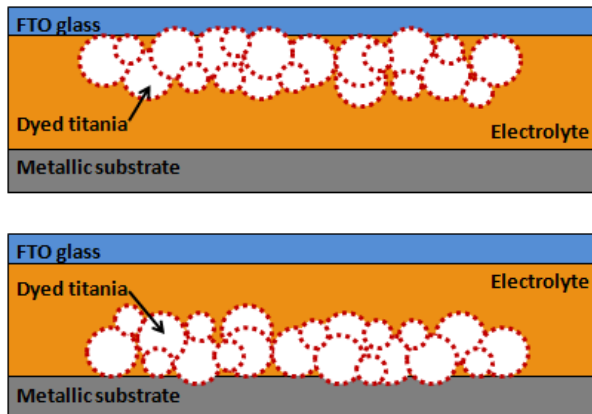


Figure 3.1: (a) front illumination and (b) back illumination configurations in which the TiO_2 film is on the FTO-glass substrate and on the metal substrate, respectively.

The counter-electrodes were prepared by depositing a drop of 5nM HPtCl_6 -propanol on the conductive surface of the substrates and firing at 450°C for 30 minutes.

The electrodes were sealed together at 125°C using a $60\mu\text{m}$ -thick thermoplastic (Surlyn-60, Dyesol) gasket. The iodide/triiodide electrolyte solution was injected in the hole drilled in the glass electrode using a fine-tip pipette. The holes were sealed using $30\mu\text{m}$ -thick thermoplastic (Surlyn-30, Dyesol) and glass pieces. Indium films acting as current collectors were soldered on the FTO face of the glass electrodes.

10 DSCs were fabricated and tested for each type of electrode, thick titanium, thin titanium and FTO-glass. In each case 5 DSCs we fabricated in the front illumination (FI) configuration and 5 in the back illumination (BI) configuration.

3.3.4 Microstructural and cell performance characterisation

The anodic layer formed by anodization and the sputtered titanium layer were characterised using a Hitachi S-4700 field emission scanning electron microscope. All the DSCs were characterized every day during 10 days using a PV Measurements Inc. A solar simulator providing $1000\text{W}/\text{m}^2$ AM1.5G equivalent light

calibrated with a reference silicon cell. The current to voltage (J - V) curves were measured using a Keithley 2000 Digital Multimeter and a Keithley SourceMeter. The electrochemical impedance spectroscopy spectra (EIS) were measured on the assembly day on 2 DSCs of each type using a VSP-potentiostat system from BioLogic under $1000\text{W}/\text{m}^2$ illumination, applying a 10mV AC signal and scanning at a frequency ranging between 400kHz and 10mHz at different applied bias. The EIS data were analysed with the Zview software.

3.4 Results & Discussion

3.4.1 Metallic electrodes characterisation

The anodization of the aluminum substrate produced a porous layer of about $2\mu\text{m}$ in thickness, resulting in a growth rate of about $70\text{nm}/\text{min}$ which is in the same order of magnitude as what is reported for oxalic acid anodization under these conditions [32-34]. The sputtered titanium thickness measured on the glass dummy samples were $835 \pm 25\text{nm}$ and $1.09 \pm 0.06\mu\text{m}$ for the two tested times, and will be called 850nm and $1.1\mu\text{m}$ from here on. Figure 3.2 shows the cross-section of a $1.1\mu\text{m}$ titanium sputtered anodized sample. This micrograph depicts that the titanium grew in a columnar manner during the sputtering, which is a common feature for films sputtered with a high sputtering rate [35-38].

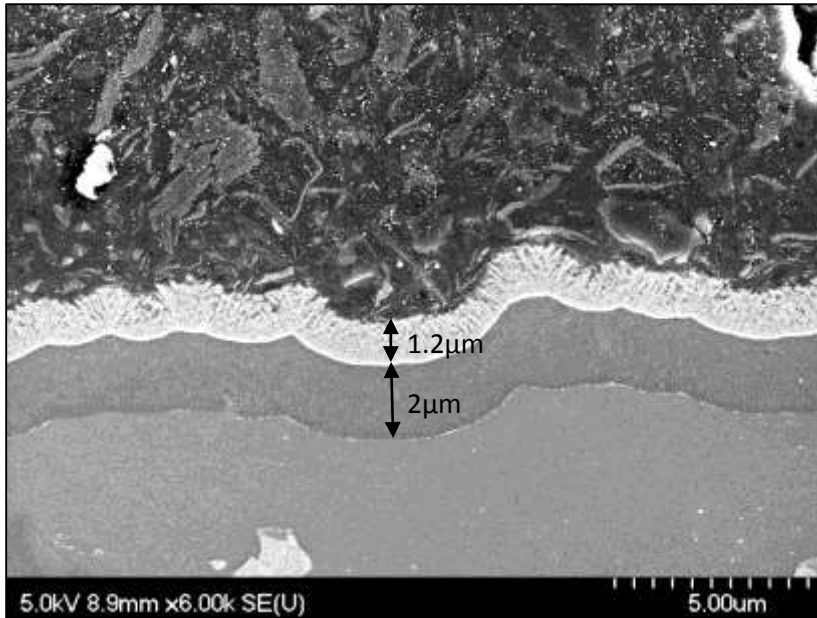


Figure 3.2: SEM cross-section of a metal substrate showing the 2 μm thick porous alumina layer and the 1.1 μm -thick sputtered titanium layer.

3.4.2 Efficiency analysis

Table 3.1 presents the average efficiencies measured on the DSCs within 30 minutes of assembly and the maximum value obtained for each type of DSC. Firstly it can be seen from these results that the DSCs based on 1.1 μm -thick titanium and the reference FTO-glass DSCs show a statistically greater average efficiency in the FI configuration than in the BI configuration. In fact these titanium-based DSCs show an average efficiency of $5.7 \pm 0.5\%$ and $2.6 \pm 0.4\%$ in the FI and BI configurations, respectively, which represents a difference of 54%. The

maximum measured values also exhibit the same trend. This behavior is expected since the incident light has to go through a layer of electrolyte before reaching the sensitized TiO₂ film in the BI configuration DSCs (see Figure 3.1). It was shown by S. Ito et al. [20] that the iodide/triiodide electrolyte cuts the incident light significantly in the range from 400nm to 600nm, thus reducing the amount of rays reaching the dye molecules and subsequently reducing the efficiency of the DSC. Moreover, the standard N719 dye has its main absorbance peak for light around 530nm [39], which is in the range of wavelengths cut by the electrolyte. On the other hand there is no significant difference in the average efficiency of DSCs based on 850nm-thick titanium between the FI and the BI configurations although a difference should be noted due to the reasons explained previously. On the other hand the maximum measured values follow the expected trend since the FI cells show a maximum conversion efficiency of 6.4% whereas BI cells show a maximum efficiency of 3.0%, a difference of 53%. This effect could come from the scatter in the efficiencies of the FI configured DSCs with 850nm-thick titanium, possibly masking the real behavior of this type of DSCs.

From the maximum efficiency results presented in Table 3.1, it is also possible to conclude that the thickness of the titanium film does not have a statistically significant effect on the efficiency of the DSCs for both the FI and the BI configuration when tested directly after fabrication. Besides, a titanium film thinner

than 850nm could also yield the same efficiency but 850nm was the minimum thickness studied in the scope of this work. Finally, the results show that all the DSCs based on metallic electrodes have a lower efficiency than the reference FTO-glass DSCs which is usually the case for other reported metal-based DSCs [16, 17, 18, 20, 22, 23].

Table 3.1: Average efficiency data for 0.175cm² masked area [40] DSCs mounted on titanium-sputtered anodized aluminum substrates or FTO-glass substrates at one sun illumination. A 0.16cm² mask was used for the efficiency measurements. The outliers were removed from the statistics (2 outliers for BI and 1 outlier for FI, both for thin Ti film).

	Thin Ti Film		Thick Ti Film		FTO-glass	
	Max efficiency	Average efficiency	Max efficiency	Average efficiency	Max efficiency	Average efficiency
Front Illumination	6.4	3.9 ± 1.8	6.3	5.7 ± 0.5	7.4	6.7 ± 0.4
Back Illumination	3.0	2.9 ± 0.2	3.1	2.6 ± 0.4	5.2	4.6 ± 0.4

Figure 3.3 shows current-voltage curves for the best DSCs with both titanium thicknesses and for both configurations, respectively. It can be seen on this graph that the best FI DSCs have a similar behavior independently of the titanium thickness. The same similarity is observed for the best BI cells. Oppositely Figure 3.3 makes it obvious that the FI DSCs show a greater overall conversion efficiency

than BIs cells due to an increase in open circuit voltage of the order of 5% accompanied by an even greater increase in short-circuit current of the order of 50%.

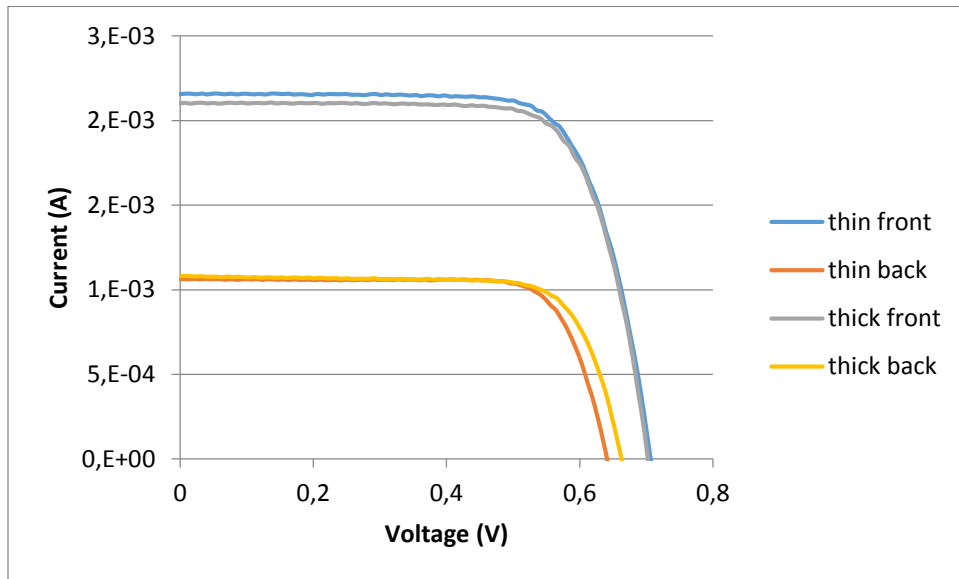


Figure 3.3: I-V curves of DSCs based on 1.1 μ m- and 850nm-thick titanium films in FI and BI configurations. A 0.16cm² mask was used for the measurements.

3.4.3 Electrochemical impedance spectroscopy analysis

Figures 3.4(a) and (b) show examples of EIS spectra of 1.1 μ m-thick and 850nm-thick based DSCs for both configurations. Using the EIS spectra and the equivalent circuit shown in Figure 3.5, the average values of resistance of the circuit could be found; the average values of R_1 , $DX1-C$ and R_s for each type of DSCs are presented in Table 3.2.

Firstly, the $R1$ component of the circuit gives information about the resistance of the metallic electrodes, depending on the configuration [41]. In the case of FI DSCs, where the metallic electrode is used as a counter-electrode, an increase in $R1$ is linked with an increase of transport resistance at the counter-electrode. For our FI DSCs the $R1$ averages are statistically similar: $7.2 \pm 1.5\Omega$ and $6.6 \pm 2.4\Omega$ for cells based on $1.1\mu\text{m}$ -thick and 850nm -thick titanium films, respectively. This means that the thickness of the sputtered titanium film does not seem to influence the transport resistance of the metallic electrodes. On the other hand, when the metallic electrode is used as an anode a rise in the $R1$ component should indicate an increase in the charge transfer resistance. Similarly, the thickness of the titanium layer has no influence as the values of $R1$ are statistically similar: $2.0 \pm 0.5\Omega$ and $2.5 \pm 0.1\Omega$ for the thick and thin titanium films based BI DSCs. This also reinforces the hypothesis that an increase in the titanium thickness from 850nm to $1.1\mu\text{m}$ does not improve the performance of the DSCs.

The $DX1-C$ component indicates the charge recombination resistance at the interface between the photoanode and the electrolyte [42, 43]. Since all the DSCs were constructed with the same TiO_2 films and the same electrolyte a similarity in the $DX1-C$ component should indicate that the thick and thin titanium films behave similarly in terms of charge recombination resistance with the I_3^- ions. It can be

seen from Table 3.2 that the values of $DX1-C$ are all in the same range, which validates the uniformity in the charge recombination resistance.

Finally, the series resistance R_s component of the circuit is an indication of the bulk resistance of the electrodes. It can be seen from Table 3.2 that the series resistance of DSCs based on 1.1 μm -thick titanium films is statistically similar to that of DSCs based on 850nm-thick titanium. This indicates that a 250nm increase in the sputtered titanium film thickness would not further increase the bulk conductivity of the film. Therefore the values of $R1$, $DX1-C$ and R_s seem to validate the fact that an increase in the titanium film thickness from 850nm to 1.1 μm does not alter the maximum achievable performance of the Ti-sputtered aluminum electrodes.

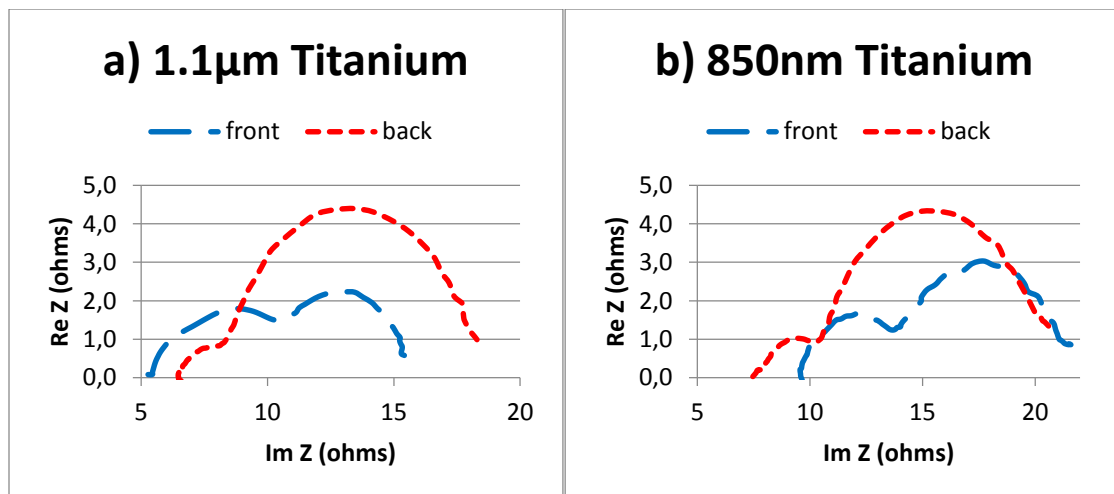


Figure 3.4: Nyquist plots of front and back illumination DSCs based on a) 1.1 μm - and b) 850nm-thick sputtered titanium substrates.

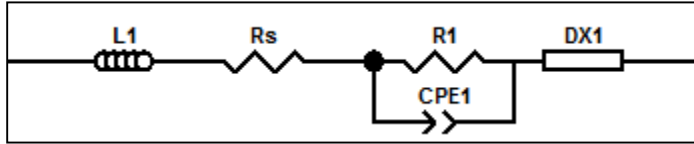


Figure 3.5: Electrochemical impedance spectroscopy equivalent circuit.

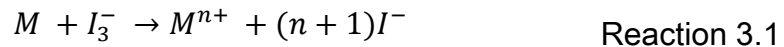
Table 3.2: Electrochemical impedance spectroscopy equivalent circuit resistance components R1, DX1-C and R_s average values per DSC type, in ohms.

	R1 (Ω)	DX1-C (Ω)	R_s (Ω)
1.1 μ m-front	7.2 \pm 1.5	9.4 \pm 1.9	5.9 \pm 0.7
1.1 μ m-back	2.0 \pm 0.5	9.2 \pm 0.1	7.3 \pm 0.9
850nm-front	6.6 \pm 2.4	12.3 \pm 2.8	8.2 \pm 1.2
850nm-back	2.5 \pm 0.1	9.3 \pm 0.5	8.9 \pm 1.1

3.4.4 Analysis of cell performance over a 10-day period

Previous work [23] have shown that polished titanium coupons and titanium foils (0.03mm thick) were found inert to the triiodide ions present in the electrolyte over a period of more than 12 weeks and 24 hours respectively, which suggest a possible stability of the current DSC over a longer period of time. In that essence, the medium-term performance of the sputtered-titanium-based DSCs was tested by measuring their efficiency daily over a period of 10 days at room temperature. The average efficiency as a function of time is shown in Figure 3.6 for 1.1 μ m titanium and glass DSCs. The FI and BI titanium-based DSCs showed a gradual

reduction in their efficiency along with a change in the color of the electrolyte from dark orange to colorless. Knowing that the triiodide ions confer the orange color to the electrolyte, this loss of color in the electrolyte was attributed to the reduction of triiodide ions to iodide ions ($I_3^- \rightarrow I^-$) [22, 25] which causes the reduction of the amount of triiodide ions present in the electrolyte solution and reduces the regeneration rate of the DSC and the cell efficiency. According to Toivola et al. [22] the reduction of triiodide ions could occur following Reaction 3.1.



The color change observed in the scope of this work indicates that a given portion of the titanium sputtered anodized aluminum electrodes react with the triiodide ions thus causing a reduction in the cell's efficiency. A possible explanation to this behavior is the surface irregularity of the sputtered films caused by the columnar growth of the films, as it was shown in Figure 2. As a matter of fact an irregular surface is more susceptible to corrosion by the electrolyte than a smooth surface due to the presence of pits that act as corrosion initiation sites [35]. Moreover the columnar structure of the films could allow the electrolyte to penetrate the titanium layer, thus significantly increasing the contact area between the rough titanium and the electrolyte and possibly even allowing the electrolyte to reach the underlying anodized aluminum substrate. Furthermore, the observation of an anodized aluminum coupon under SEM after heating at 450°C for 30 minutes allowed to see

that the alumina layer, which is supposed to protect the aluminum, cracked due to the different thermal expansion coefficients of aluminum and alumina. The surface of the cracked alumina layer is shown on Figure 3.7. Since 450°C is the sintering temperature of the TiO₂ films and of the platinum all the metal-based electrodes used as photo-anodes and as counter-electrodes should exhibit cracks allowing the electrolyte to reach the exposed aluminum. Thus, this reaction could be responsible for the efficiency loss suffered by our metallic-electrode-based DSCs. Since the color of the electrolyte did not change in the glass DSCs this reduction of triiodide is attributed to the presence of metallic electrodes.

Glass DSCs also exhibited a decrease in their efficiency, as shown in Figure 3.6, without any apparent change in the electrolyte color. This efficiency loss is attributed to the evaporation of the volatile electrolyte. The rate of evaporation of the electrolyte varied for every glass-based DSC due to the manual sealing of each DSC separately. Since all the DSCs studied were assembled using the same procedure it is possible to conclude that the decrease in efficiency observed in the case of metal-based DSCs is mainly caused by the reduction of the amount of triiodide ions in the electrolyte, but also is supplemented by some evaporation of the electrolyte. Nevertheless this efficiency degradation rate is comparable to that of the study of K. Miettunen et al. where the efficiency of DSCs based on stainless steel photo-anodes drops by 90% in two weeks [15]. No corrosion reaction was

reported but it was found that the stainless steel photo-electrode could affect the TiO₂ film thus reducing the conversion efficiency.

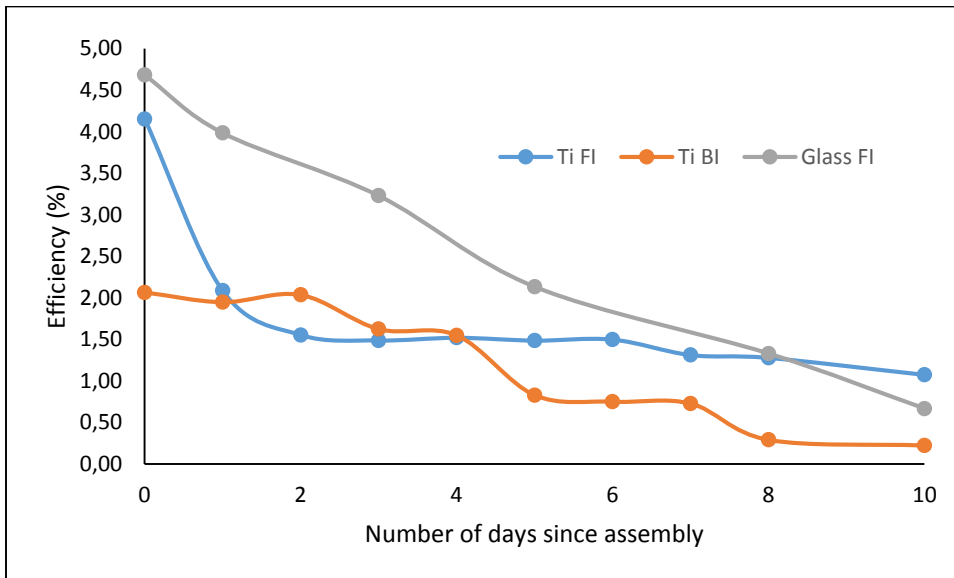


Figure 3.6: Efficiency degradation curves of the front and back illumination DSCs made with 1.1 μ m-thick sputtered titanium substrates and of the FI reference DSC made on FTO-glass electrodes. The efficiency values were measured without masking for consistency.

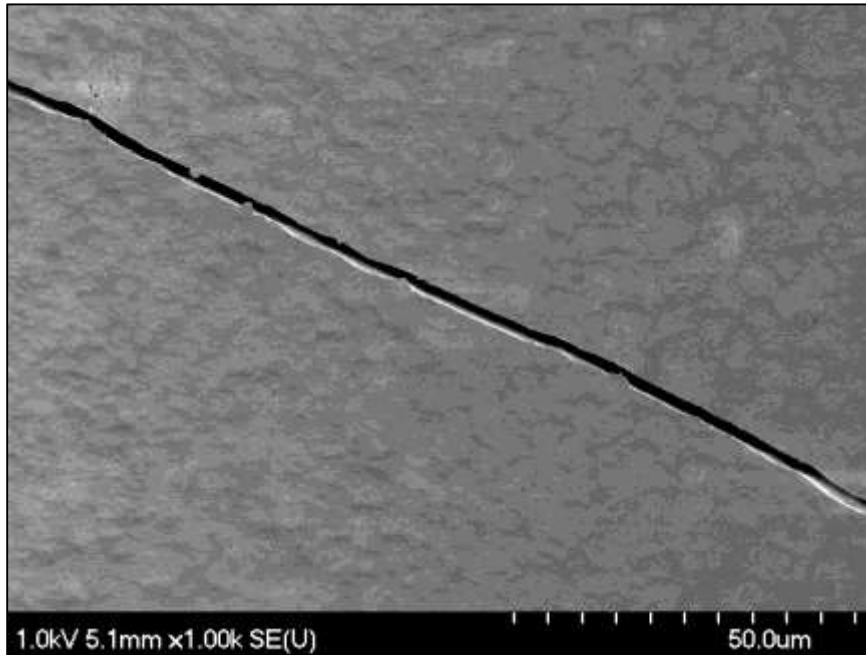


Figure 3.7: SEM picture of a crack seen at the surface of an anodized aluminum coupon after heating at 450°C for 30 minutes.

3.4.5 Efficiency comparison

Table 3.3 compares the current results with reported values for other metal-based BI DSCs. As shown, the efficiency values obtained in this study are comparable to the other metallic systems. Firstly, a comparison with other titanium-based DSCs is presented. Watson et al. [17] have prepared BI DSCs based on titanium coupons and on pre-painted aluminised steel sputtered with 1.2 μm of titanium and obtained maximum efficiencies of 3.2% and 2.9%, respectively. Also, K. Miettunen et al. [23] have prepared BI DSCs directly onto titanium foils and have obtained a maximum efficiency of 3.4%. These values are similar to the 2.9% and 2.6% average

efficiencies obtained for the BI DSCs fabricated in this study with 850nm and 1.1 μ m titanium films respectively. Finally, the research group of S. Ito et al. [20] have managed to fabricate a BI DSC based on a titanium foil resulting in a high maximum efficiency of 7.2%. This high efficiency is partly attributed to the good fabrication conditions of their lab as their reference FI glass DSC showed an important efficiency of 9.9%.

K. Miettunen et al. [23] also used Inconel and stainless steel as photo-anodes obtaining 2.8% efficiency in both cases. These efficiencies are lower than the 3.4% efficiency obtained on titanium foils in the same paper as described earlier. Other stainless steel based BI DSCs were fabricated by Y. Jun et al. [18] Layers of ITO and SiO_x were sputtered on the stainless steel substrates allowing them to achieve a maximum efficiency of 6.1%.

Table 3.3: Comparison table of BI DSCs based on metallic electrodes. The Glass Ref column states the efficiency of the glass reference DSCs fabricated in the same studies whether it is “higher” or “lower” than the metal-based DSC. N/A in the masking area column indicates that this information was not mentioned.

Authors	Metallic Electrode	η	Masking Area	Year	Glass Reference
M.-P. Cote et al.	1.1 μm -thick titanium sputtered anodized aluminum	2.6%	0.16 cm^2	2013	4.6%
This work	850nm-thick titanium sputtered anodized aluminum	2.9%			
T.M. Watson et al. [17]	Pre-painted aluminised steel sputtered with titanium titanium coupon	2.9% 3.2%	N/A	2011	higher
K. Miettunen et al. [23]	Stainless steel Inconel titanium foil	2.8% 2.8% 3.4%	Slightly greater than active area.	2010	4.6%
Y. Jun et al. [18]	ITO and SiO_x sputtered stainless steel	6.1%	N/A	2007	higher
S. Ito et al. [20]	Titanium foil	7.2%	N/A	2006	9.9%

FI DSCs have also been fabricated in the scope of our study allowing to increase the average efficiency of the 850nm and 1.1 μm thick titanium film DSCs to 3.9% and 5.7%, respectively. Other research groups have used metals as counter-electrodes for DSCs. The results are presented in Table 3.4. Including all metallic electrode systems considered, the highest efficiency was obtained by J.H. Park et

al. [24] by sputtering layers of SiO_x and ITO on stainless steel substrates and by spin coating titanium-isopropoxide (TIP) onto the surface prior to TiO₂ deposition. The highest efficiency obtained is ~ 8.6%. C.M. Chen et al. [19] have also used stainless steel as base material for DSCs electrodes allowing them to reach efficiencies of 6.4% and 7.0% with as-prepared and etched stainless steel electrodes, respectively. Nickel-based DSCs with a maximum efficiency of 7.3% have also been fabricated in the scope of their research. M. Toivola et al. [22] and T. Ma et al. [16] also published papers on stainless steel based DSCs with efficiencies of 3.6% and 5.2%, respectively. This difference in efficiency is consistent with the maximum efficiencies reported by these two groups for their reference glass-based cells being 4.6% and 6.0%, respectively. Carbon steel was also used by M. Toivola et al. [22] giving 3.1% efficiency and T. Ma et al. [16] used nickel as a counter-electrode resulting in an efficiency of 5.1%. At last, J. WeiWei et al. [21] have published results for DSCs based on glass substrates with evaporated aluminum and sputtered platinum layers. Using this electrode as a counter-electrode gave a maximum efficiency of 7.1% which is more than double the efficiency of their reference glass DSC of 3.5%- a result that raises questions as to accuracy of their measurements.

Finally, apart from the results reported by J. WeiWei et al. [21] it is possible to see from the data shown in Table 3.3 and Table 3.4 that it is common to obtain greater efficiencies for glass-based reference DSCs than for metal-based DSCs.

Table 3.4: Comparison table of FI DSCs based on metallic electrodes. The Glass Ref column states the efficiency of the glass reference DSCs fabricated in the same whether it is “higher” or “lower” than the metal-based DSC. N/A in the masking area column indicates that this information was not mentioned.

Authors	Metallic Electrode	η	Masking Area	Year	Glass Reference
M.-P. Cote et al.	1.1 μm -thick titanium sputtered anodized aluminum	5.7%	0.16 cm^2	2013	6.7%
	This work	3.9%			
C.-M. Chen et al. [19]	Nickel	7.3%	N/A	2010	-
	Stainless steel	6.4%			
	Etched stainless steel	7.0%			
J. WeiWei et al. [21]	Platinum-sputtered aluminum-evaporated glass	7.1%	N/A	2009	3.5%
J.H. Park et al. [24]	Titanium-isopropoxide-treated stainless steel	8.6%	N/A	2008	-
M. Toivola et al. [22]	Stainless steel	3.6%	N/A	2006	4.6%
	Carbon steel	3.1%			
T. Ma et al. [16]	Stainless steel	5.2%	N/A	2004	6.0%
	Nickel	5.1%			

3.5 Conclusion

This work has shown that DSCs can be manufactured onto titanium-sputtered anodized aluminum coupons. Maximum efficiencies of 6.4% and 6.3% were achieved with 850nm and 1.1 μ m titanium-based cells, respectively. These values are approaching the maximum efficiency obtained on reference FTO-glass cells being 7.4%. On the other hand the metal-based DSCs exhibit a rapid degradation due to the combined effects of the reaction of the electrolyte with the metallic electrode and the evaporation of the electrolyte. Therefore, further work needs to be done in order to ameliorate the stability of the titanium-based DSCs but their initial performance makes them a suitable alternative to develop to the currently rigid and costly TCO-glass based cells.

3.6 References

1. B. O'Regan and M. Gratzel. A low-cost, high-efficiency solar-cell based on dye-sensitized colloidal TiO₂ films. *Nature* 1991; 353: 737.
2. M.K. Nazeeruddin et al. Conversion of light to electricity by cis-X₂bis(2,2'-bipyridyl-4,4'-dicarboxylate)ruthenium(II) charge-transfer sensitizers (X=Cl⁻, Br⁻, I⁻, CN⁻, and SCN⁻) on nanocrystalline TiO₂ electrodes. *Journal of American Chemical Society* 1993; 115: 6382.
3. C.J. Barbé et al. Nanocrystalline titanium oxide electrodes for photovoltaic applications. *Journal of the American Ceramic Society* 1997; 80: 3157.
4. M.K. Nazeeruddin et al. Engineering of efficient panchromatic sensitizers for nanocrystalline TiO₂-based solar cells. *Journal of the American Chemical Society* 2001; 123: 1613.
5. H. Geiger et al. Environmental aspects of electricity generation from a nanocrystalline dye sensitized solar cell system. *Renewable Energy* 2003; 23: 1613.
6. G. Smestad, C. Bignozzi and R. Argazzi. Testing of dye sensitized TiO₂ solar cells I: experimental photocurrent output and conversion efficiencies. *Solar Energy Materials and Solar Cells* 1994; 32: 259.
7. H.J. Snaith. Estimating the maximum attainable efficiency in dye-sensitized solar cells. *Advanced Functional Materials* 2010; 20: 13.
8. M.A. Green. The path to 25% silicon solar cell efficiency: history of silicon cell evolution. *Progress in Photovoltaics: Research and Applications* 2009; 17: 183.
9. W.A. Gazotti et al. Flexible photoelectrochemical devices based on conducting polymers. *Synthetic Metals* 2000; 108: 151.
10. H. Lindstrom et al. A new method to make dye-sensitized nanocrystalline solar cells at room temperature. *Journal of Photochemistry and Photobiology A: Chemistry* 2001; 145: 107.

11. G. Boschloo et al. Optimization of dye-sensitized solar cells prepared by compression method. *Journal of Photochemistry and Photobiology A: Chemistry* 2002; 148: 11.
12. C. Longo et al. Solid-state and flexible dye-sensitized TiO₂ solar cells: a study by electrochemical impedance spectroscopy. *Journal of Physical Chemistry B* 2002; 106: 5925.
13. C. Longo, J. Freitas and M.-A. De Paoli. Performance and stability of TiO₂/dye solar cells assembled with flexible electrodes and a polymer electrolyte. *Journal of Photochemistry and Photobiology A: Chemistry* 2003; 159: 33.
14. M. Ikegami et al. Platinum/titanium bilayer deposited on polymer film as efficient counter electrodes for plastic dye-sensitized solar cells. *Applied Physics Letters* 2007; 90: 153122-1.
15. K. Miettunen, J. Halme and P. Lund. Segmented cell design for improved factoring of aging effects in dye solar cells. *Journal of Physical Chemistry C* 2009; 113: 10297.
16. T. Ma et al. Properties of several types of novel counter electrodes for dye-sensitized solar cells. *Journal of Electroanalytical Chemistry* 2004; 574: 77.
17. T.M. Watson, G.J. Reynolds and D.A. Worsley. Painted steel mounted dye sensitised solar cells: titanium metallisation using magnetron sputtering. *Ironmaking and Steelmaking* 2011; 38: 168.
18. Y. Jun, J. Kim and M.G. Kang. A study of stainless steel-based dye-sensitized solar cells and modules. *Solar Energy Materials & Solar Cells* 2007; 91: 779.
19. C.-M. Chen, C.-H. Chen and T.-C. Wei. Chemical deposition of platinum on metallic sheets as counterelectrodes for dye-sensitized solar cells. *Electrochimica Acta* 2010; 55: 1687.

20. S. Ito et al. High-efficiency (7.2%) flexible dye-sensitized solar cells with Ti-metal substrate for monocrystalline-TiO₂ photoanode. *Chemical Communications* 2006: 4004.
21. J. WeiWei et al. A new type counter electrode for dye-sensitized solar cells. *Science in China Series E: Technological Sciences* 2009; 52: 1923.
22. M. Toivola, F. Ahlskog and P. Lund. Industrial sheet metals for nanocrystalline dye-sensitized solar cell structures. *Solar Energy Materials & Solar Cells* 2006; 90: 2881.
23. K. Miettunen et al. Stability of dye solar cells with photoelectrode on metal substrates. *Journal of the Electrochemical Society* 2010; 157: B814.
24. J.H. Park et al. Fabrication of an efficient dye-sensitized solar cell with stainless steel substrate. *Journal of the Electrochemical Society* 2008; 155: F145.
25. G.J. Reynolds et al. Corrosion resistance of metallic substrates for the fabrication dye-sensitized solar cells. *Journal of the Electrochemical Society* 2011; 33: 129.
26. J.M. Kroon et al. Nanocrystalline dye-sensitized solar cells having maximum performance. *Progress in Photovoltaics: Research and Applications* 2007; 15: 1.
27. M.J. de Wild-Scholten and A.C. Veltkamp. Environmental life cycle analysis of dye sensitized solar devices; status and outlook. *ECN Solar Energy*.
28. S. Roberts and N. Guariento, *Building Integrated Photovoltaics A Handbook*. Birkhauser, Boston (2009), p. 7-12.
29. www.aluminum.org
30. J.R. Davis, *Aluminum and Aluminum Alloys* (4th edition). ASM International (1993), p.1-784.
31. European Aluminum Association Factsheet, http://www.aluminium-award.eu/2009/upload/files/EAA_building_09_2008.pdf.

32. P. Chowdhury et al. Effect of process parameters on growth rate and diameter of nano-porous alumina templates. *Bulletin of Materials Science* 2011; 34: 423.
33. C. Cheng, K.Y. Ng and A.H.W. Ngan. Quantitative characterization of acid concentration and temperature dependent self-ordering conditions of anodic porous alumina. *AIP Advances* 2011; 1: 042113.
34. C.H. Voon et al. Effect of temperature of oxalic acid on the fabrication of porous anodic alumina from Al-Mn alloys. *Journal of Nanomaterials* 2013; 2013: 1.
35. S. Yang et al. Influence of columnar microstructure of a sputtered NiAl coating on its oxidation behavior at 1000°C. *Intermetallics* 2002; 10: 467.
36. R. Nedelec et al. Dense yttria-stabilised zirconia electrolyte layers for SOFC by reactive magnetron sputtering. *Journal of Power Sources* 2012; 205: 157.
37. S.L. Lee et al. Analysis of magnetron-sputtered tantalum coatings versus electrochemically deposited tantalum from molten salt. *Surface and Coatings Technology* 1999; 120-121: 44.
38. F. Ruske et al. Hydrogen doping of DC sputtered ZnO:Al films from novel target material. *Surface & Coatings Technology* 2005; 200: 236.
39. Y. Chiba et al. 15th International Photovoltaic Science & Engineering Conference (PVSEC-15), Shanghai, China, 2005. Technical Digest: 665.
40. H.J. Snaith. The perils of solar cell efficiency measurements. *Nature Photonics* 2012; 6: 337.
41. K.E. Lee et al. Enhanced surface hydroxylation of nanocrystalline anatase films improves photocurrent output and electron lifetime in dye sensitized solar cell photoanodes. *Electrochimica Acta* 2012; 67: 208.
42. J. Bisquert. Theory of the impedance of electron diffusion and recombination in a thin layer. *Journal of Physical Chemistry B* 2002; 106: 325.

43. R. Kern et al. Modeling and interpretation of electrical impedance spectra of dye solar cells operated under open-circuit conditions. *Electrochimica Acta*; 47: 4213.

Chapter 4. Molybdenum- and ITO-Sputtered Anodized Aluminum Substrates

In the previous chapter proof-of-concept results were presented demonstrating the use of Ti-sputtered anodized aluminum as a substrate in fabricating electrodes for DSCs. Since titanium is an expensive metal it was decided to investigate alternate to titanium conductive films. To this end molybdenum- and indium tin oxide-sputtered anodized substrates were prepared and tested as counter electrodes.

The results of this investigation presented in this chapter are destined for publication in the near future. The following provides the current citation information:

M.-P. Cote, G.P. Demopoulos and M. Brochu, "Molybdenum- and ITO-Sputtered Anodized Aluminum Substrates". *Article intended for publication.*

2013

4.1 Abstract

Molybdenum and ITO films were sputtered onto anodized aluminum coupons. The latter sputtered coupons were successfully used as counter-electrodes substrates in DSCs. The average efficiency of the front-illumination DSCs based on molybdenum and ITO are 3.7% and 1.5%, respectively. The lower photovoltaic performance of ITO-based cells is attributed to their higher internal resistance than molybdenum-based DSCs, as confirmed by EIS analysis. Therefore molybdenum is considered as a better option than ITO for DSCs application.

4.2 Introduction

Since their invention in 1991 by O'Regan and Gratzel, dye-sensitized solar cells (DSCs) have attracted a lot of attention because of their simplicity in fabrication, potentially low cost of production, relatively high theoretical light-to-electricity conversion and their ability to generate electricity under a wide range of lighting conditions [1-6]. They also attract a lot of attention as they can be made flexible and can be fabricated as building integrated parts and portable devices. This is in line with the efforts to replace the conventional transparent conductive oxide (TCO) glass by either polymeric [7-11] or metallic [12-23] electrodes. Replacing the commonly used TCO-glass by another material would also render the DSCs more economically and environmentally friendly. Indeed, TCO-glass represents a major

part of the cost of DSCs [5, 24] and is the component that is the most detrimental to the environment [4, 25].

Steel [13, 20, 21, 23] and titanium [21, 23] have already been used as substrate materials in DSCs. Particularly, companies such as Dyesol and Tata Steel have worked towards stainless steel-based building integrated DSCs [26]. On the other hand aluminum is nearly absent from the DSC scene despite the fact that it is the second most widely used material in the world [27]. This absence is blamed on the need to anodize aluminum for outdoor applications in order to improve its corrosion resistance. Anodizing creates a surface oxide layer that is responsible for this enhanced property. Unfortunately, the insulating properties of Al_2O_3 [28] prevent the conduction of the electrons through the oxide layer and through the metal electrode thus making it arduous to use in DSCs.

In order to use aluminum as DSCs electrodes, thin conductive films can be sputtered on the anodized aluminum samples. This structure is similar to conductive glass where a conductive layer, usually a TCO, is deposited on the insulator substrate, glass. Although TCO-glass is a common choice for electrodes fabrication other substrates based on the same structure have recently been developed, molybdenum-coated glass is one of them [29, 30]. In a companion paper (Chapter 3) the use of Ti-sputtered anodized aluminum as substrate for fabricating DSC electrodes was investigated. The scope of this research is to

demonstrate the possibility of using sputtered molybdenum and indium-tin oxide (ITO) on anodized aluminum substrates to mimic the structure of TCO- or molybdenum-coated glass substrates. In the present case, the aluminum-based electrodes were used as counter-electrodes along with FTO glass-based photo-anodes. The photovoltaic characteristics of the molybdenum- and ITO-based DSCs are presented.

4.3 Experimental

4.3.1 Aluminum substrate

An AA 1100 plate with a thickness of 3.2mm was cut in 4.5 by 2.5cm coupons to be used as the base material for the electrodes preparation. In order to eliminate surface defects created during rolling and handling, the coupons were ground down to 1200 grit grinding paper. Next, the coupons were pre-treated by dipping in a 2.5M sodium hydroxide solution at 55°C for 30 seconds to etch the native alumina layer and subsequently dipping in a 2.4M nitric acid solution at room temperature to 30 seconds to improve the surface finish. After each pre-treatment step the coupons were rinsed with water and methanol and dried. The pre-treated samples were then anodized over a 9cm² area in 0.3M oxalic acid at 20°C under a potential of 30V for 30 minutes.

4.3.2 Conductive layer sputtering

The anodized aluminum substrates were cleaned with methanol prior to sputtering. The molybdenum and ITO films were sputtered on the samples using a Denton E14 DC sputterer. The deposition conditions are shown in Table 4.1. Final thicknesses of 1.1 μ m and 500nm were targeted for the molybdenum and ITO films, respectively. The actual values were determined by measuring the film thickness on a glass dummy samples using a stylus profilometer. These anodized-aluminum substrates sputtered with molybdenum and ITO will simply be called molybdenum and ITO substrates from now on.

Table 4.1: Deposition conditions for molybdenum and ITO sputtering with Denton E14 DC.

Material	DC/RF	Gas	Pressure (mTorr)	Power (W)	Current (A)	Deposition Rate ($\text{\AA}/\text{s}$)
Mo	DC	Argon	10	-	1.1	1.75
ITO	RF	Argon	4.9	200	-	1.75

4.3.3 DSC fabrication

Prior to cell fabrication, holes were drilled in the FTO-glass substrates, which were then cleaned with micro-90 soap in an ultrasonic bath for 30 minutes and further rinsed with ethanol and dried. The metal substrates were simply wiped with ethanol.

A 50 μm thick mask with an area of 1 cm^2 was applied on the conductive surface of the 2.5 by 4.5cm FTO-glass substrates. A TiO_2 paste (Dyesol 18NRT) was applied using the doctor blading technique and sintered at 450 $^\circ\text{C}$ for 30 minutes after removal of the mask. The thickness of the TiO_2 films was measured using a stylus profilometer and only the anodes with a TiO_2 film thickness between 8 and 12 μm were further used. The glass-based photo-anodes were then immersed in a 40mM TiCl_4 solution at 75 $^\circ\text{C}$ for 30 minutes and subsequently rinsed with distilled water and sintered at 450 $^\circ\text{C}$ for 30 minutes. Finally, the anodes were immersed in a ruthenium-based dye (N719, Dyesol) for 24h. The now sensitized anodes were rinsed with ethanol and dried and were assembled immediately.

The metallic counter-electrodes were prepared by depositing a drop of 5nM HPtCl_6 -propanol on the surface of the molybdenum and ITO films and firing for 30 minutes. The counter-electrodes based on ITO were fired at 450 $^\circ\text{C}$ but the molybdenum electrodes were fired at 300 $^\circ\text{C}$ to avoid oxidation of the conductive film. 300 $^\circ\text{C}$ was experimentally found to be the minimum temperature at which the platinum was activated but 450 $^\circ\text{C}$ is the optimal temperature [31].

The electrodes were sealed together at 125 $^\circ\text{C}$ using a 60 μm -thick thermoplastic (Surlyn-60, Dyesol) gasket. The iodide/triiodide electrolyte solution was injected in

the hole drilled in the glass electrode using a fine-tip pipette. The holes were sealed using 30 μ m-thick thermoplastic (Surlyn-30, Dyesol) and glass pieces. Indium films acting as current collectors were soldered on the FTO face of the glass electrodes. Three DSCs were fabricated and tested for each thin film material. The final structure of the DSCs is shown in Figure 4.1.

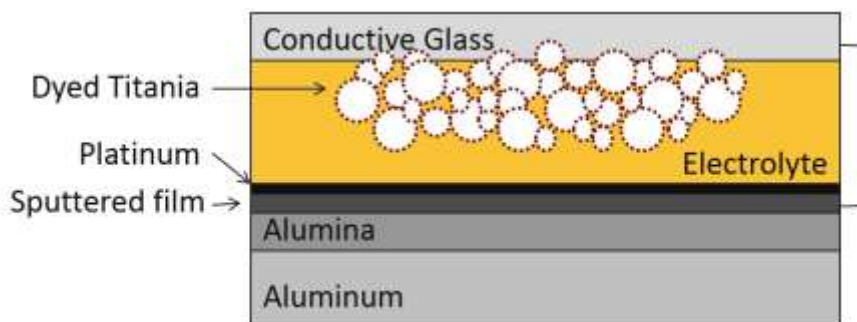


Figure 4.1: Schematic of the thin conductive film counter electrode-based DSC configuration.

4.3.4 Electrodes and DSC characterisation

The anodic layer formed by anodization in oxalic acid and the sputtered molybdenum and ITO layers were characterised using an Hitachi S-3700N scanning electron microscope. The DSCs were characterized within 30 minutes of assembly using a PV Measurements Inc. solar simulator providing 1000W/m² AM1.5G equivalent light calibrated with a reference silicon cell. The current to voltage ($J-V$) curves were measured using a Keithley 2000 Digital Multimeter and

a Keithley SourceMeter. For these measurements the active surface of the DSCs was masked to show an area of 0.16cm^2 [32]. The electrochemical impedance spectroscopy (EIS) spectra were measured using a VSP-potentiostat system from BioLogic under 1000W/m^2 illumination, applying a 10mV AC signal and scanning at a frequency ranging between 400kHz and 10mHz at different applied bias. The EIS data were analysed with the Z-View software.

4.4 Results & Discussion

The anodization process produced a porous layer of about $2\mu\text{m}$ in thickness, resulting in a growth rate of about 70nm/min which is in the same order of magnitude as what is reported for oxalic acid anodization under these conditions [33-35]. The sputtered thicknesses measured on the glass dummy samples were $1200 \pm 20\text{nm}$ and $450 \pm 8\text{nm}$ for molybdenum and ITO, respectively. Figure 4.2 shows an example of the structure of the electrodes substrates, in this case molybdenum-sputtered anodized alumina samples.

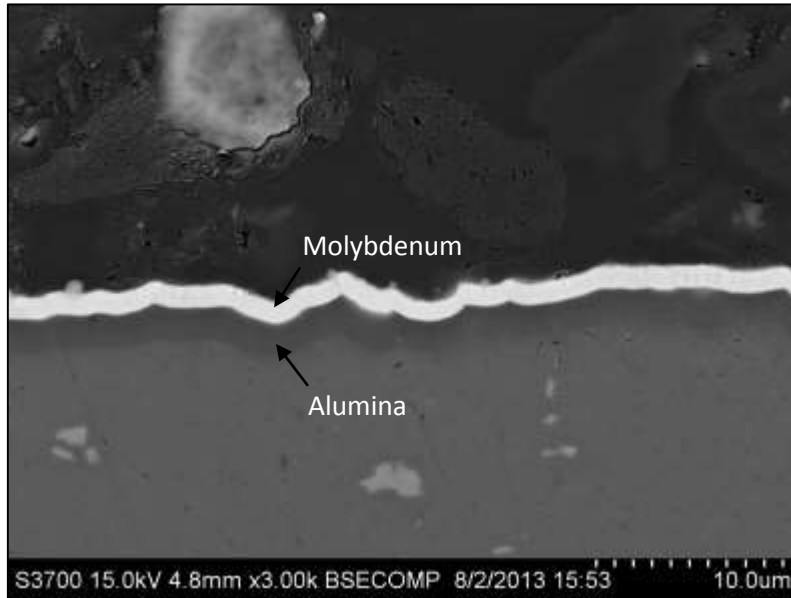


Figure 4.2: SEM picture of the cross-section of a molybdenum-sputtered anodized aluminum substrate showing the 2 μm -thick alumina layer and the 1.2 μm -thick molybdenum layer.

Table 4.2 reports the average characteristics of 3 DSCs for each type of electrode in terms of short-circuit current (J_{sc}), open circuit voltage (V_{oc}), fill factor (FF) and overall conversion efficiency (η). It can be seen from these results that the average values of short-circuit current and open circuit voltage are similar for both types of DSCs. In fact the J_{sc} values are 9.2 ± 2.1 and $9.7 \pm 2.9 \text{ mA/cm}^2$ and the V_{oc} values are 531 ± 46 and $555 \pm 56 \text{ mV}$ for molybdenum and ITO, respectively. Oppositely, the average fill factor of molybdenum-based cells is $75 \pm 3\%$ which is almost three times greater than that of ITO-based cells ($28 \pm 2\%$). Since a high internal resistance is known to decrease the fill factor [16, 19] this difference indicates that

ITO-sputtered electrodes could be more resistive than molybdenum-sputtered electrodes. This difference in fill factor ultimately influences the overall conversion efficiency going from $3.7 \pm 1.0\%$ for molybdenum-based DSCs to $1.5 \pm 0.4\%$ for ITO-based DSCs.

This behavior can be seen in Figure 4.3 showing the I-V curves of the best DSCs of each type. It can be seen on this graph that the two curves have different shapes, the molybdenum-based cell showing a more squared curve whereas the ITO-based cell shows a curve that approaches a straight line.

Table 4.2: Mo- and ITO-based DSCs short-circuit current (J_{sc}), open-circuit voltage (V_{oc}), fill factor (FF) and efficiency (η).

	J_{sc} (mA/cm ²)	V_{oc} (mV)	FF (%)	η (%)
Mo	9.2 ± 2.1	531 ± 46	75 ± 3	3.7 ± 1.0
ITO	9.7 ± 2.9	555 ± 56	28 ± 2	1.5 ± 0.4

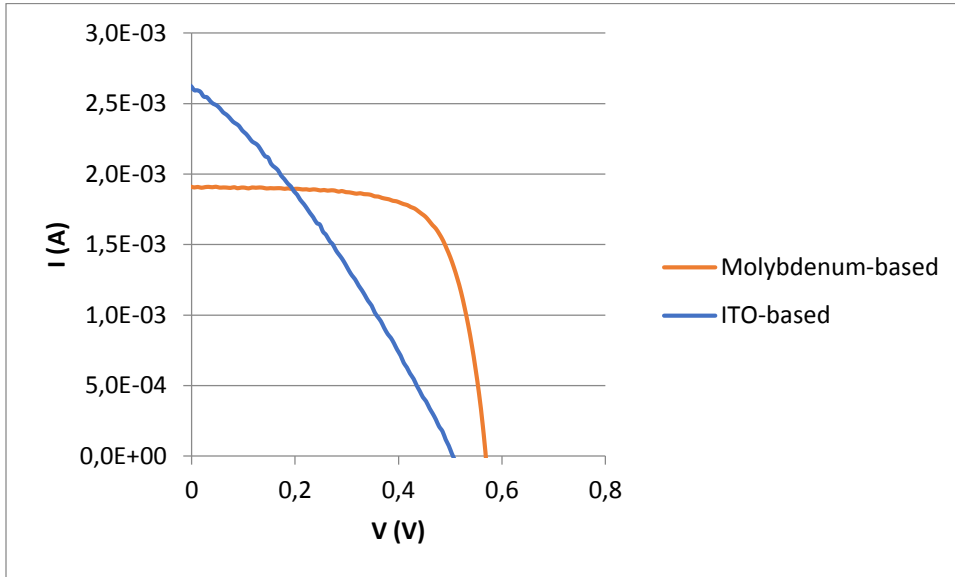


Figure 4.3: Comparison of the I-V curves of ITO- and molybdenum-based front illumination configured DSCs.

In order to explain the low fill factor of ITO-based DSCs electrochemical impedance spectroscopy was performed on all the molybdenum- and ITO-based cells. Figure 4.4 shows examples of Nyquist plots for the best DSCs of each type. Using the Nyquist plots and the equivalent circuit shown in Figure 4.5 the resistance components of the DSCs were determined with Z-view software. Table 4.3 summarizes the results obtained.

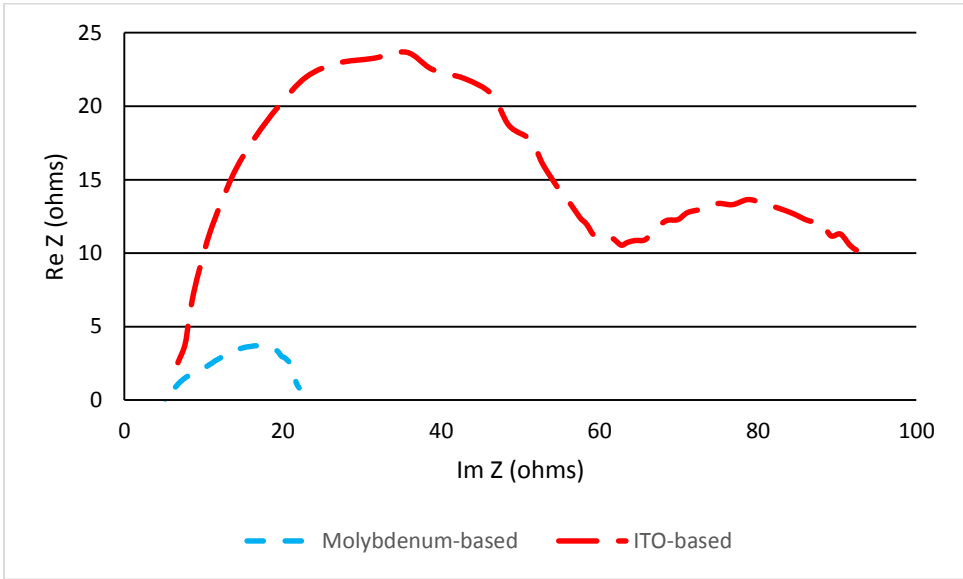


Figure 4.4: Nyquist plots of molybdenum- and ITO-based DSCs

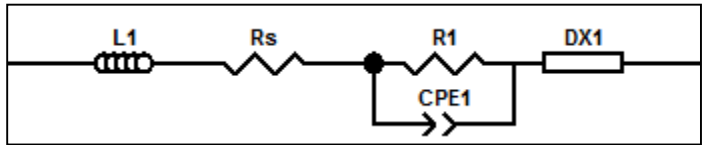


Figure 4.5: Electrochemical impedance spectroscopy equivalent circuit.

Table 4.3: R_s and $R1$ component of the equivalent circuit shown in Figure 4.5 for Mo- and ITO-based DSCs EIS.

	$R_s(\Omega)$	$R1(\Omega)$
Mo	7.8 ± 2.5	7.1 ± 5.0
ITO	6.7 ± 0.3	119 ± 67

The impedance spectroscopy analysis shows that the bulk resistance of the electrodes are similar for molybdenum- and ITO-based DSCs since the values of R_s are similar: 7.8 ± 2.5 and $6.7 \pm 0.3\Omega$, respectively. Oppositely the values of $R1$ are significantly greater for ITO-based cells than for molybdenum-based cells: 119 ± 67 for ITO in comparison to 7.1 ± 5.0 for molybdenum. Since this term represents the transport resistance at the counter-electrode and the charge transfer resistance at the photo-anode [36], it is logical to conclude that the internal resistance of the ITO-based DSCs is much greater than that of molybdenum-based DSCs. Moreover since all the photo-anodes were made in the same conditions on identical FTO-glass substrates this difference must come from a higher transport resistance at the surface of the ITO-sputtered electrode. This higher resistance for ITO-based electrodes is coherent with the bulk resistivity of ITO that is about 40 times greater than that of molybdenum. Additionally it is conceivable that the composition of the ITO film was not uniform resulting in even higher loss of conductivity.

Considering the obtained efficiency and the internal resistance of the cells, the ease of fabrication and cost/material abundance, when we compare Mo and ITO, it is concluded that molybdenum is a viable candidate for sputtering anodized-aluminum-based DSC electrodes. Therefore further work is warranted towards the optimization and further testing of the Mo-sputtered electrodes.

4.5 Conclusion

This work has shown that both molybdenum and ITO can be used as sputtered conductive films on anodized aluminum for DSCs electrodes with the former being superior to the latter. Efficiencies of $3.7 \pm 1.0\%$ and $1.5 \pm 0.4\%$ have been achieved using electrodes sputtered with 1.1 μm -thick molybdenum and 850nm-thick ITO, respectively. The lower efficiency of ITO-based cells was linked via EIS analysis to the high surface transport resistance of the sputtered film apparently arising from poor film composition uniformity hence low conductivity. Molybdenum electrodes on the other hand seem to be a good candidate for DSC application and further R&D work is recommended as it can successfully unleash the potential of using aluminum widely in PV applications.

4.6 References

1. B. O'Regan and M. Gratzel. A low-cost, high-efficiency solar-cell based on dye-sensitized colloidal TiO₂ films. *Nature* 1991; 353: 737.
2. M.K. Nazeeruddin et al. Conversion of light to electricity by cis-X₂bis(2,2'-bipyridyl-4,4'-dicarboxylate)ruthenium(II) charge-transfer sensitizers (X=Cl⁻, Br⁻, I⁻, CN⁻, and SCN⁻) on nanocrystalline TiO₂ electrodes. *Journal of American Chemical Society* 1993; 115: 6382.
3. C.J. Barbé et al. Nanocrystalline titanium oxide electrodes for photovoltaic applications. *Journal of the American Ceramic Society* 1997; 80: 3157.
4. H. Geiger et al. Environmental aspects of electricity generation from a nanocrystalline dye sensitized solar cell system. *Renewable Energy* 2003; 23: 1613.
5. G. Smestad, C. Bignozzi and R. Argazzi. Testing of dye sensitized TiO₂ solar cells I: experimental photocurrent output and conversion efficiencies. *Solar Energy Materials and Solar Cells* 1994; 32: 259.
6. H.J. Snaith. Estimating the maximum attainable efficiency in dye-sensitized solar cells. *Advanced Functional Materials* 2010; 20: 13.
7. W.A. Gazotti et al. Flexible photoelectrochemical devices based on conducting polymers. *Synthetic Metals* 2000; 108: 151.
8. H. Lindstrom et al. A new method to make dye-sensitized nanocrystalline solar cells at room temperature. *Journal of Photochemistry and Photobiology A: Chemistry* 2001; 145: 107.
9. G. Boschloo et al. Optimization of dye-sensitized solar cells prepared by compression method. *Journal of Photochemistry and Photobiology A: Chemistry* 2002; 148: 11.
10. C. Longo et al. Solid-state and flexible dye-sensitized TiO₂ solar cells: a study by electrochemical impedance spectroscopy. *Journal of Physical Chemistry B* 2002; 106: 5925.

11. C. Longo, J. Freitas and M.-A. De Paoli. Performance and stability of TiO₂/dye solar cells assembled with flexible electrodes and a polymer electrolyte. *Journal of Photochemistry and Photobiology A: Chemistry* 2003; 159: 33.
12. M. Ikegami et al. Platinum/titanium bilayer deposited on polymer film as efficient counter electrodes for plastic dye-sensitized solar cells. *Applied Physics Letters* 2007; 90: 153122-1.
13. K. Miettunen, J. Halme and P. Lund. Segmented cell design for improved factoring of aging effects in dye solar cells. *Journal of Physical Chemistry C* 2009; 113: 10297.
14. T. Ma et al. Properties of several types of novel counter electrodes for dye-sensitized solar cells. *Journal of Electroanalytical Chemistry* 2004; 574: 77.
15. T.M. Watson, G.J. Reynolds and D.A. Worsley. Painted steel mounted dye sensitised solar cells: titanium metallisation using magnetron sputtering. *Ironmaking and Steelmaking* 2011; 38: 168.
16. Y. Jun, J. Kim and M.G. Kang. A study of stainless steel-based dye-sensitized solar cells and modules. *Solar Energy Materials & Solar Cells* 2007; 91: 779.
17. C.-M. Chen, C.-H. Chen and T.-C. Wei. Chemical deposition of platinum on metallic sheets as counterelectrodes for dye-sensitized solar cells. *Electrochimica Acta* 2010; 55: 1687.
18. S. Ito et al. High-efficiency (7.2%) flexible dye-sensitized solar cells with Ti-metal substrate for monocrystalline-TiO₂ photoanode. *Chemical Communications* 2006: 4004.
19. J. WeiWei et al. A new type counter electrode for dye-sensitized solar cells. *Science in China Series E: Technological Sciences* 2009; 52: 1923.
20. M. Toivola, F. Ahlskog and P. Lund. Industrial sheet metals for nanocrystalline dye-sensitized solar cell structures. *Solar Energy Materials & Solar Cells* 2006; 90: 2881.

21. K. Miettunen et al. Stability of dye solar cells with photoelectrode on metal substrates. *Journal of the Electrochemical Society* 2010; 157: B814.
22. J.H. Park et al. Fabrication of an efficient dye-sensitized solar cell with stainless steel substrate. *Journal of the Electrochemical Society* 2008; 155: F145.
23. G.J. Reynolds et al. Corrosion resistance of metallic substrates for the fabrication dye-sensitized solar cells. *Journal of the Electrochemical Society* 2011; 33: 129.
24. J.M. Kroon et al. Nanocrystalline dye-sensitized solar cells having maximum performance. *Progress in Photovoltaics: Research and Applications* 2007; 15: 1.
25. M.J. de Wild-Scholten and A.C. Veltkamp. Environmental life cycle analysis of dye sensitized solar devices; status and outlook. *ECN Solar Energy*.
26. Tata Steel. 2011 Sustainable energy solutions. See http://www.tatasteeleurope.com/en/responsibility/sustainable_solutions/energy/.
27. www.aluminum.org
28. J.R. Davis, *Aluminum and Aluminum Alloys* (4th edition). ASM International (1993), p.1-784.
29. www.guardian.com
30. www.saint-gobain-solar-power.com
31. P.M. Sommeling et al. Influence of a TiCl_4 post-treatment on nanocrystalline TiO_2 films in dye-sensitized solar cells. *Journal of Physical Chemistry B* 2006; 110: 19191.
32. H.J. Snaith. The perils of solar cell efficiency measurements. *Nature Photonics* 2012; 6: 337.

33. P. Chowdhury et al. Effect of process parameters on growth rate and diameter of nano-porous alumina templates. *Bulletin of Materials Science* 2011; 34: 423.
34. C. Cheng, K.Y. Ng and A.H.W. Ngan. Quantitative characterization of acid concentration and temperature dependent self-ordering conditions of anodic porous alumina. *AIP Advances* 2011; 1: 042113.
35. C.H. Voon et al. Effect of temperature of oxalic acid on the fabrication of porous anodic alumina from Al-Mn alloys. *Journal of Nanomaterials* 2013; 2013: 1.
36. K.E. Lee et al. Enhanced surface hydroxylation of nanocrystalline anatase films improves photocurrent output and electron lifetime in dye sensitized solar cell photoanodes. *Electrochimica Acta* 2012; 67: 208.

Chapter 5. Summary

It was shown in Chapter 3 and Chapter 4 that anodized aluminum coupons sputtered with titanium, ITO or molybdenum can in principle be used as counter-electrodes and photo-anodes (only for the case of titanium) in DSCs. The best front illumination results were obtained with DSCs based on titanium sputtered films; the maximum efficiencies obtained were equivalent for cells based on 850nm and 1.1 μ m thick titanium films. The molybdenum-based cells were found to be less efficient than titanium-based DSCs but still more efficient than ITO-based DSCs. The higher resistance of the sputtered ITO films was shown to be responsible for this reported lower efficiency.

Back illumination DSCs based on titanium films were also studied in Chapter 3 and were shown to exhibit a lower efficiency than front illumination cells based on the same substrates. This behavior was expected and was also observed on the FTO-glass reference cells.

Finally, Chapter 3 has also shown that although the initial efficiency of titanium-based DSCs is competitive with that of glass-based DSCs their instability in time remains a major issue. The reasons for this decrease in efficiency were identified

as the evaporation of the electrolyte because of problems with the sealing of a metal-based DSC and its reaction with the metallic electrode.

Overall, because of their higher efficiency and their lower internal resistance but also cost and availability of materials (In being a rare and expensive metal), titanium- and molybdenum-sputtered DSCs are the most promising type of DSCs based on aluminum coupons studied in this work. But since the reaction of the electrolyte with the metallic electrodes remains an issue the replacement of this electrolyte with a less corrosive one could be a great continuation to this project. As a matter of fact work towards this direction has been undertaken recently by a few research groups [1-4]. For example an all-solid-state electrolyte has been developed in 2012 by I. Chung et al [4]. By using their solution-processable semiconductor CsSnI_3 in lieu of a liquid electrolyte they obtained an overall conversion efficiency of 8.5%. When the efficiency of solid-state DSCs remained low because of poor filling of the porous TiO_2 film the solution-processable electrolyte developed by this group can make intimate contact with the dye molecules and the TiO_2 particles, explaining the great performance of the DSCs. In addition to eliminating the reaction problem between the electrolyte and the metallic substrates the use of solid-state electrolyte could eliminate sealing issues, thus solving the main problems faced in the scope of this work.

5.1 References

1. J.-H. Yum et al. A cobalt complex redox shuttle for dye-sensitized solar cells with high open-circuit potentials. *Nature Communications* 2012; 3:1.
2. M. Wang et al. An organic redox electrolyte to rival triiodide/iodide in dye-sensitized solar cells. *Nature Chemistry* 2010; 2: 385.
3. J.K. Koh et al. Highly efficient, iodine-free dye-sensitized solar cells with solid-state synthesis of conducting polymers. *Advanced Materials* 2011; 23: 1641.
4. I.Chung et al. All-solid-state dye-sensitized solar cells with high efficiency. *Nature* 2012; 485: 486.